AMERICAN SCIENTIFIC PUBLISHERS

Science of Advanced Materials
Vol. 7, pp. 1916–1944, 2015
www.aspbs.com/sam

REVIEW

Graphene-Based Composites for Supercapacitor Electrodes

Xiaohua Fan[1,2,3], Bruce D. Phebus[2], Lingjie Li[3], and Shaowei Chen[2,*]

[1]*School of Safety Engineering, Chongqing University of Science and Technology, Shapingba District, Chongqing 401331, China*
[2]*Department of Chemistry and Biochemistry, University of California, Santa Cruz, California 95064, USA*
[3]*College of Chemistry and Chemical Engineering, Chongqing University, Shapingba District, Chongqing 400030, China*

ABSTRACT

Graphene is a promising electrode material for supercapacitors (SCs) due to its large specific surface area, high electrical conductivity, and chemical and mechanical stability. It is a single-atom thick substrate that may be used for the growth of functional nanomaterials and can have synergistic effects with other materials to greatly improve the specific capacitance of SCs. Recently, numerous studies have been carried out with graphene-based composites as SC electrodes. In this article, we will first review briefly the parameters and factors that affect the performance of SCs, and then discuss various types of graphene-based composite materials for SC electrodes, including graphene–conducting polymer composites, graphene–transition metal oxides/hydroxides/sulfide composites, graphene–heteroatoms composites, graphene–other carbonaceous nanomaterial composites, and graphene-based ternary composites. Lastly, the perspective of the critical issues for high performance SCs based on graphene composites will be discussed.

KEYWORDS: Graphene, Composites, Supercapacitor Electrode, Conducting Polymers, Transition Metal Oxides.

CONTENTS

1. INTRODUCTION

Supercapacitors (SCs) are one of the alternative energy storage devices being proposed to power the future, due to their high power performance, long cycle life and low maintenance costs. However, because the energy densities of SCs is much lower than batteries, their applications are limited.[1] Energy density is the ability to store energy and it determines how long the SCs can act as a power source. The energy storage capability of the SCs is represented by the equation below,[2]

$$E = \frac{1}{2}CV^2 \quad (1)$$

where C represents the capacitance and V is the cell voltage. According to the equation, the energy density of SCs can be enhanced by either increasing the device capacitance with novel electrode materials or broadening the cell voltage. Usually, the cell voltage can be increased by two ways: (a) using ionic liquids or organic electrolytes because of their wider potential windows than aqueous electrolytes;[3,4] (b) taking advantage of asymmetric SCs, which integrate the different potential windows of the positive electrode and negative electrode to increase the operation voltage.[5–9] Meanwhile, the device capacitance can be increased by various methods: (a) developing materials with a large accessible surface area, such as hierarchical nanostructured or nanoporous materials;[10,11] (b) improving the wetting of electrodes by electrolytes;[12,13] (c) enhancing mass transport;[14] (d) high mass loading and effective utilization of active materials (Fig. 1).[14,15]

*Author to whom correspondence should be addressed.
Email: shaowei@ucsc.edu
Received: 7 October 2014
Accepted: 1 November 2014

That is, the performance of SCs depends strongly on the properties of electrode materials and their relative configurations.

There are two energy storage mechanisms utilized in SCs such that the SCs are classified into two types by their electrode materials,[1, 16, 17] electric double layer capacitors (EDLCs) and pseudo-capacitors (PCs). EDLCs store energy via ion adsorption/desorption on the electrode surface, exhibit an excellent cycle life and power density but are hampered by limited adsorption capacity which impacts energy density.[14] Carbon materials with a large specific surface area and excellent electrical conductivity, such as active carbon (AC), carbon nanotubes (CNTs), and graphene, have been used for EDLCs. In contrast, PCs store energy via fast reversible surface redox reactions. Typical pseudo-capacitive materials include transition metal oxides/hydroxides and conducting polymers. They hold a much higher energy density but unsatisfactory cycle stability and rate capability, so power density is in general low (Fig. 2, Table I).[14]

Power density represents how fast energy can be discharged or charged, which is another important

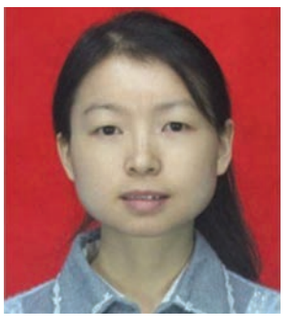

Xiaohua Fan is a lecturer in the College of Safety Engineering, Chongqing University of Science and Technology, China. She received her Master's degree in applied chemistry at Chongqing University in 2007 and has been pursuing a Ph.D. degree at the same University under the supervision of Professor Lingjie Li since 2011. Her major research interest entails the synthesis of graphene-based materials and their applications.

Bruce D. Phebus received his B.S. degree from San Jose State University in 2006 working under Professor Roger Terrill on solid-state conduction of fluorozirconate glass. He then worked under Drs. Laura Iraci and Brad Stone at NASA Ames and received his M.S. degree for work on the nucleation of water ice clouds on Mars in 2009. He is currently working toward his Ph.D. degree at UCSC under the direction of Professor Shaowei Chen. His research interest is primarily in the synthesis, engineering and chemical sensing of carbon nanomaterials.

Lingjie Li studied applied chemistry and physical chemistry at Chongqing University, and obtained her bachelor and master's degrees in 1996 and 1999, respectively. She studied materials science at Beijing University of Aeronautics and Astronautics and obtained her Ph.D. degree in 2002. From 2002 to 2004 she worked as a postdoctoral fellow at Lawrence Berkeley National Laboratory, USA. Since 2004 she has been a full professor at the School of Chemistry and Chemical Engineering, Chongqing University. Her current research interests cover electrochemistry and materials science at the micro/nanoscale, with a particular focus on corrosion and surface engineering of metals and alloys.

Shaowei Chen finished his undergraduate studies in China in 1991 with a B.Sc. degree in Chemistry from the University of Science and Technology of China, and then went to Cornell University receiving his M.Sc. and Ph.D. degrees in 1993 and 1996, respectively. Following a postdoctoral appointment in the University of North Carolina at Chapel Hill, he started his independent career in Southern Illinois University in 1998. In summer 2004, he moved to the University of California at Santa Cruz and is currently a Professor of Chemistry. His research interest is primarily in the electron transfer chemistry of nanoparticle materials.

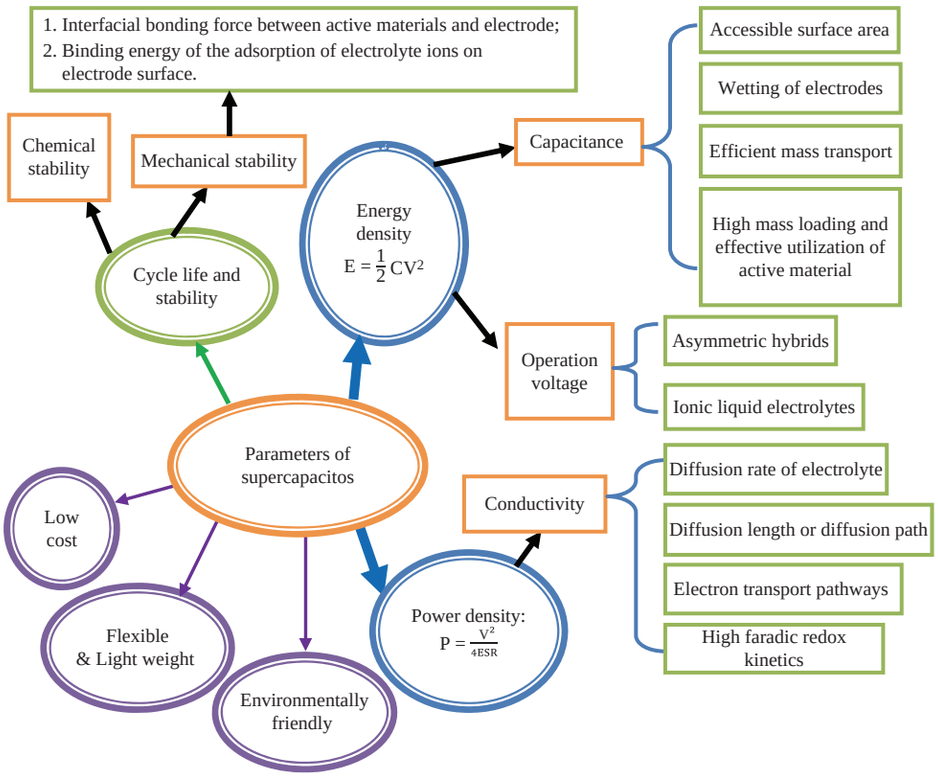

Fig. 1. Parameters and factors that affect the performance of SCs.

parameter of SCs. It can be represented by the equation below,[2]

$$P = \frac{V^2}{4\mathrm{ESR}} \tag{2}$$

where V is the operation voltage and ESR is the equivalent series resistance. Therefore, another effective way to improve power density is to reduce the resistance of the electrode. This may be realized by developing electrode materials with a short diffusion distance, rich electron transport pathways, and high electronic conductivity.[18, 19]

A major challenge is to improve energy densities of SCs while simultaneously to retain their high power densities and cycle stability.[1, 20, 21] Of course, other parameters, such as low cost, flexibility, light weight and environmental friendliness, are also important for SCs.

Graphene is a two dimensional single layer of sp2 hybridized carbon atoms with a hexagonal structure. It has

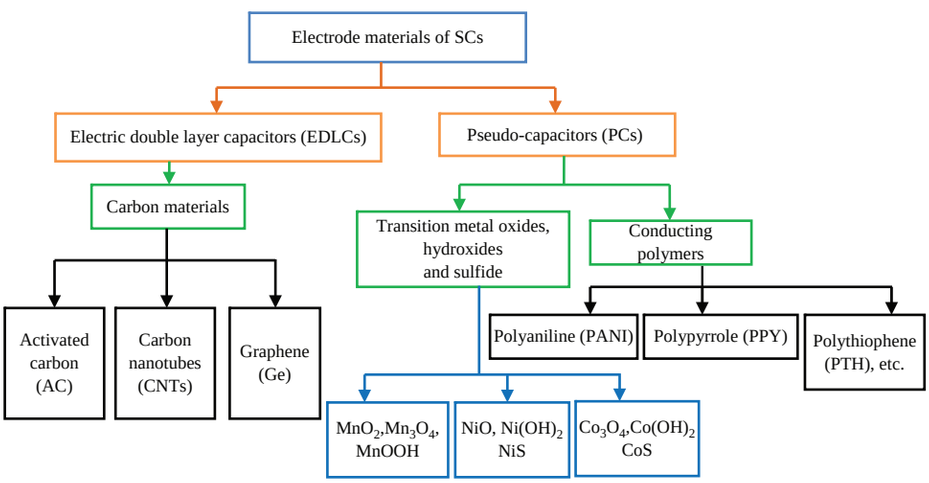

Fig. 2. Main electrode materials of SCs.

REVIEW

Table I. Summary and comparison of SCs electrode materials.

SCs electrode materials	Advantages	Disadvantages
Electrical double layer capacitors (EDLCs) AC, CNTs, etc.	Large specific surface area; High power density.	Weak interfacial bonding; Low capacitance; Lower energy densities.
Graphene	Large theoretical surface area; Good electronic conductivity; High stability; High power density.	Aggregation or re-stacking of graphene nanosheets; Lower energy densities
Pseudo-Capacitors (PCs) Transition metal oxides/hydroxides	High specific capacitances; High energy density.	Low operating voltage; high costs; Poor electrical conductivity; Inefficient mass transport; Poor rate capability; slow faradic redox kinetics; Mechanical deformation in the redox process, poor; Life-cycle stability; Low power density.
Conducting polymers	High specific capacitances; High energy density.	Poor electrical conductivity; Poor rate performance; Mechanical deformation in the redox process, poor life-cycle stability;

been hailed as an ideal electrode material for EDLCs due to its exceptional properties, such as superior electrical conductivity and mechanical strength, extremely high theoretical surface area (2630 $m^2 \cdot g^{-1}$), and excellent theoretical capacitance (550 $F \cdot g^{-1}$).[22] However, the electrochemical performance of graphene is far from the theoretical expectation because its high tendency to restack between neighboring sheets owing to the strong interlayer van der Waals force.[23] This results in the deterioration of its high specific surface area and subsequent decrease in specific capacitance. Tremendous effort has been exerted to overcome this problem, and one promising strategy is to incorporate graphene with other functional (nano) materials to form effective composites and use them as SC electrode materials, such as conducting polymers (e.g., polyaniline, polypyrrole),[24, 25] transition metal oxides/hydroxides (e.g.,NiO, MnO_2, $Co(OH)_2$),[26–28] heteroatoms (e.g., N, B and O),[29, 30] and other carbonaceous nanomaterials (e.g., AC, CNTs).[14, 31] Numerous reports have shown that rational design and synthesis of these graphene-based composites cannot only prevent the restacking of graphene and improve the specific capacitance of EDLCs but also greatly improve the total specific capacitance of the electrode, because graphene is a single-atom thick substrate that may be exploited for the growth of functional nanomaterials to render them electrochemically active and electrically conductive (Fig. 3).

In this review article we survey the recent advances in research and development of graphene-based composites that are used as SCs electrode materials. We will mainly focus on graphene-conducting polymer composites, graphene-transition metal oxides/hydroxides/sulfide composites, graphene-heteroatoms composites, graphene-other carbonaceous nanomaterials composites, and graphene-based ternary composites. Lastly, the perspective of the future development of high performance SCs based on graphene composites are proposed.

2. GRAPHENE-CONDUCTING POLYMERS NANOCOMPOSITES

Conducting polymers (CPs) are a promising material for the fabrication of high performance SCs, due to their high specific capacity, low band gap, suitable morphology, fast kinetics of charge/discharge processes and low costs. Polyaniline, polypyrrole, polythiophene, and their derivatives have been the most commonly studied polymers in this regard.[32] However, CPs suffers from poor cycling stability caused by swelling and shrinking of the polymer backbones during charging/discharging, which greatly hinder their practical applications.

In order to overcome this drawback, considerable effort has been directed toward the synthesis of graphene-CP nanocomposites, because graphene has good conductivity, stable physicochemical properties, and long cycle life, so the conductivity and cyclic stability of the composites will be improved significantly. The CPs not only provide pseudo-capacitance but also improve the wetting between graphene and electrolytes due to their hydrophilic nature.[33] In addition, the unique two-dimensional structure of graphene not only provides electrochemical double-layer capacitance, but also acts as an effective substrate to facilitate facile electrochemical reactions of CPs leading to highly reversible pseudo-capacitance.[32]

2.1. Graphene-Polyaniline Composites

Among the CPs, Polyaniline (PANI) has been most widely studied, due to its high capacitance, good environmental stability, high flexibility, multi-redox states, acid-based doping/dedoping chemistry, low costs, easy synthesis, and so on. Unfortunately, rapid structural degradation occurs during successive charge/discharge process because of swelling and shrinkage arising from adsorption and desorption of electrolyte ions. In addition, the relatively low conductivity results in a poor rate performance and cycling stability that greatly restricts practical applications

REVIEW

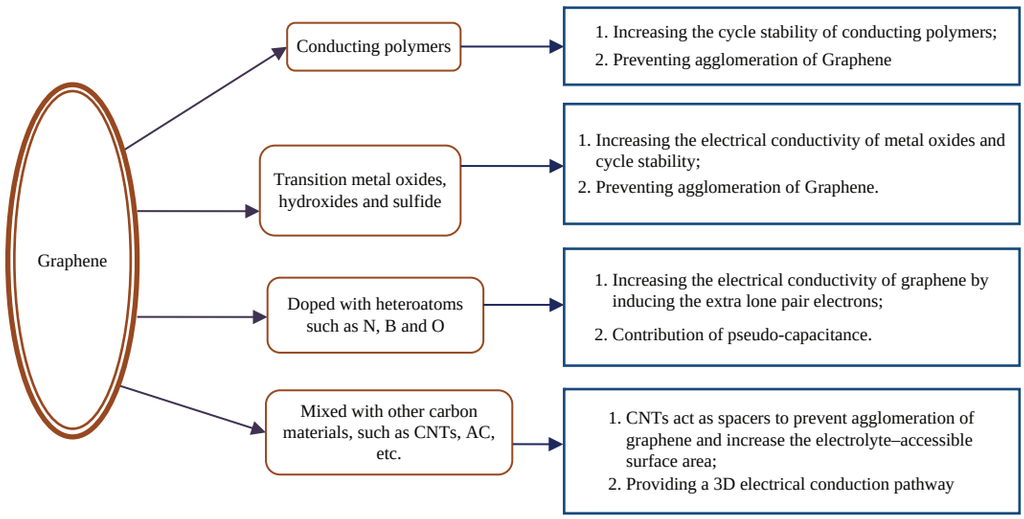

Fig. 3. Graphene-based composites and the corresponding mechanism of their electrochemical performance.

in SCs.[34–36] The incorporation of graphene with PANI has been proven to not only reinforce the stability and conductivity of PANI, but also to significantly improve its capacitance performance.[35]

Various approaches have been developed to fabricate graphene-PANI nanocomposites, such as *in-situ* and *ex-situ* polymerization,[37] covalent and non-covalent bonding interactions,[36] template technique and three-dimensional (3D) structure,[38] and so on.

In the earlier studies, graphene-PANI composites were mostly prepared by physical mixing, but the specific capacitance was generally very low, possibly due to the poor interconnection between graphene and PANI.[39] More recently, graphene-PANI composites are usually fabricated by *in-situ* polymerization in the presence of aniline monomers and graphene suspension using graphene as a substrate. PANI nanoparticles homogeneously grow onto the surfaces of the graphene sheets and act as spacers to keep neighboring sheets from restacking onto one another.[37, 39] However, as both sides of the graphene sheets are covered with PANI, it is not favorable to form effective conducting networks among the composites as the graphene sheets do not have direct contact with each other. Partial aggregation of graphene sheets may hinder both diffusion as well as reduce the available surface area, therefore, the specific capacitance and rate capability are still unsatisfactory.[35]

There are several methods that have been used to fabricate 3D graphene-PANI composities. Kulkarni et al. used 3D graphene structures that contained interconnected pores to prevent the restacking of graphene sheets, which not only provides a large surface area for a high loading of PANI, but also offers a highly continuous conducting network for charge transfer.[40] This led to significant improvement of the SC performances. Sachin et al. produced PANI nanofibers/3D graphene frameworks by using a chemical vapor deposition (CVD) and template method.[40] Firstly, the 3D graphene frameworks were prepared via CVD growth of graphene on a Ni foam, followed by Ni etching. Nanofibrous PANI were then deposited onto the 3D graphene via chemical oxidative polymerization in an aqueous solution containing aniline or anilinium salts, using ammonium persulfate as an oxidizing agent. The maximum specific capacitance of the PANI/3D graphene electrode was found to be 1024 $F \cdot g^{-1}$.

In addition to Ni foam which has been widely used as a sacrificial template to produce 3D porous structures, polymer microspheres and inorganic liquid droplets or micelles have also been used as sacrificial templates which include materials such as Teflon,[41] polystyrene sulfonate microsphere (PSS),[42] mesoporous silica,[35] $CaCO_3$ particles,[38] and so on. In contrast to inorganic templates, the dissolution of polymer microspheres normally needs a large amount of organic solvents. Meng et al. preapred a hierarchical porous reduced graphene oxide (rGO)/PANI composite film using $CaCO_3$ particles as a sacrificial template.[38] They found that $CaCO_3$ could be removed easily by a dilute acidic solution, and the 3D composite film displayed high flexibility and might be free-standing, which could be directly used as an electrode (Fig. 4).

CVD, dip coating, and layer-by-layer (LBL) assembly techniques can also be combined with template methods to fabricate 3D graphene/PANI hybrid.[42] Mu et al. synthesized a graphene/PANI hybrid using a hollow microspheres structure based on polystyrene sulfonate microsphere templates, by combining LBL assembly with *in situ* chemical oxidative polymerization followed by etching the templates.[42] They concluded that the unique structure provided an enhanced specific surface area and reduced transport lengths for both mass and charge transport, and so displayed high specific capacitance and good cycle stability (Fig. 5).

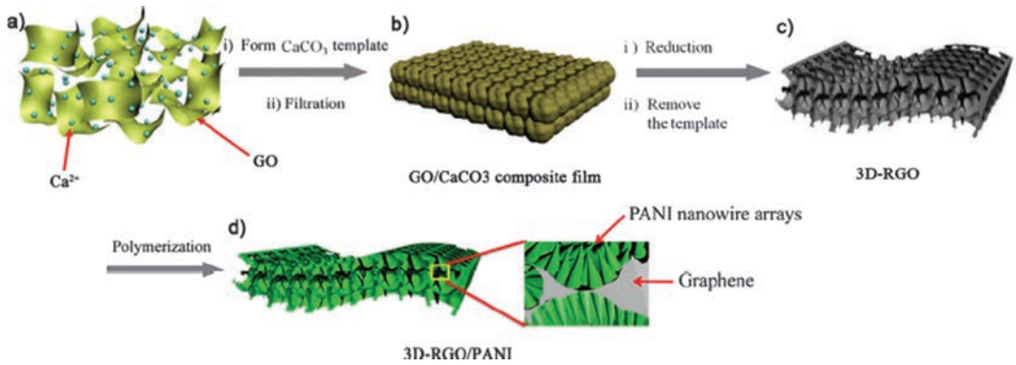

Fig. 4. Preparation of the flexible 3D-RGO and 3D-RGO/PANI films. Reproduced with permission from [38], Y. Meng, et al., *Adv. Mater.* 25, 6985 (**2013**). © 2013, Wiley-VCH Verlag GmbH & Co. KGaA, Weinheim.

Apart from the template method, 3D porous graphene structures can also be fabricated by spray drying graphene suspensions or reducing graphene oxide (GO) powders under vacuum followed by heating.[34, 43] The obtained 3D graphene is then used as a template to synthesize graphene/PANI composites by *in situ* polymerization of aniline. Although the specific capacitance was substantially increased, much room remained for improvement (Table II).

One possible reason why they fell short of expectation is that these 3D graphene structures were mainly stacked randomly, and PANI was also randomly grown on the graphene surface. In contrast, ordered PANI nanowires could reduce the diffusion path length, facilitate ionic motion, and improve utilization of electrode materials.[36] Graphene-PANI composites with ordered structure can be connected by non-covalent bonds such as van der Waals force, electrostatic interaction, π–π stacking, and covalent bonds.[44] For instance, Liu et al. prepared a 3D highly ordered structural graphene/PANI bulk hybrid for SCs.[45] Firstly, sulfonated triazine was used as functional molecules adsorbed onto graphene sheets via hydrogen bonding as well as π–π stacking interactions. Secondly, the PANI nanorods were anchored on the functional graphene nanosheets via *in situ* chemical oxidative polymerization of aniline in aqueous solution. The obtained highly ordered structural composites possessed a specific capacitance as high as 1225 $F \cdot g^{-1}$. The authors deduced that with sulfonated triazine, the functional graphene might be dispersed in water and improved the nucleation of PANI. By electrostatic interactions the PANI nanorods nucleated heterogeneously and subsequently grew vertically on the graphene surfaces (Fig. 6).

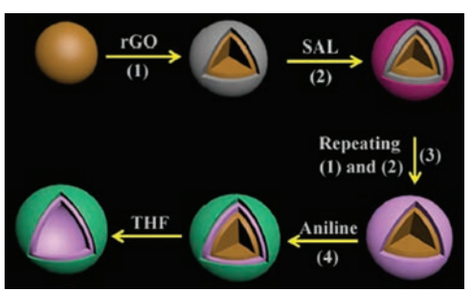

Fig. 5. Illustration of the preparation of graphene/PANI hybrid hollow microspheres combining LBL assembly technique with *in situ* chemical oxidative polymerization. Reproduced with permission from [42], B. Mu, et al., *J. Nanopart. Res.* 16 (**2014**). © 2014, Springer.

Compared to non-covalent connections, the covalent connection between PANI and graphene is expected to enhance the electrical conductivity and stability of the composites.[36, 46] For instance, Wang et al. synthesized a hierarchical graphene composite with PANI nanowire arrays covalently bonded to rGO[36] by first grafting nitrophenyl groups to rGO via C–C bonds. The nitrophenyl groups were then reduced to aminophenyl and acted as anchor sites for the vertical growth of PANI arrays (Fig. 7). The prepared composites exhibited unusually high cycling stability, showing no loss of capacitance after 200 cycles. This is a very interesting study as it illustrates the possibility of ultra-stable SCs by preparing functionalized graphene-PANI via *in situ* polymerization and covalent grafting.

Compared with graphene, GO allows ready fabrication of composite materials due to the presence of various oxygenated groups, because aqueous GO shows good compatibility with hydrophilic PANI, and increases the rate of interactions between electrolytes and electrodes. This is attributed to the polar oxygen-containing functional groups (epoxide hydroxyl, carboxyl, etc.) which render GO strongly hydrophilic and dispersible with enhanced wetting between electrodes and electrolytes. Moreover, the existing surface functionalities on GO can contribute pseudo-capacitance when used as SCs electrodes.[47, 48] Therefore, the overall electrochemical performance of GO-PANI composites may be substantially strengthened. In fact, some efforts have been directed towards the synthesis of functional GO-PANI composites. For instance, Li et al. prepared covalently-grafted PANI-GO nanocomposites by *in situ* polymerization.[24] The prepared covalently-bonded GO-PANI composites exhibited enhanced performance as

Table II. Summary of SC performance of graphene/PANI composites.

Preparation method	Electrode configuration	Electrolyte	Measurement protocol	Maximum capacitance ($F \cdot g^{-1}$)	Capacitance retention	Ref. (year)
Simple mixing of GO and PANI followed by reduction	3-electrode	1 M H_2SO_4	CV (0.1 $A \cdot g^{-1}$)	257	98% (1000 cycles)	[39] (2013)
Non-3D	3-electrode	1 M H_2SO_4	CV (5 $mV \cdot s^{-1}$)	329.5	61% (1000 cycles)	[37] (2012)
3D, Teflon template, dip coating	3-electrode	1 M H_2SO_4	CV (10 $mV \cdot s^{-1}$)	763	82% (1000 cycles)	[41] (2013)
3D, CVD, Ni foam template	3-electrode	1 M H_2SO_4	CV (10 $mV \cdot s^{-1}$)	1024	86.5% (5000 cycles)	[40] (2014)
3D, SiO_2 template	3-electrode	1 M H_2SO_4	CV (0.5 $A \cdot g^{-1}$)	749	88% (1000 cycles)	[35] (2014)
3D, $CaCO_3$ articles template, 3D, flexible, free-standing	2-electrode	1 M H_2SO_4	CV (0.5 $A \cdot g^{-1}$)	385	88% (5000 cycles)	[38] (2013)
3D, Reducing GO under vacuum followed by heating	3-electrode	1 M KOH	CV (1 $mV \cdot s^{-1}$)	463	90.6% (500 cycles)	[43] (2013)
3D, polystyrene sulfonate microsphere template, LBL assembly	3-electrode	1 M H_2SO_4	CV (10 $mV \cdot s^{-1}$)	633	92% (1000 cycles)	[42] (2014)
3D, highly ordered structure	3-electrode	1 M H_2SO_4	CV (1 $A \cdot g^{-1}$)	1225	85.7% (1500 cycles)	[45] (2014)
Covalently-grafted on RGO	3-electrode	2 M H_2SO_4	CV (0.1 $A \cdot g^{-1}$)	590	100% (200 cycles)	[36] (2013)
Covalently-grafted on graphene, interfacial copolymerization	3-electrode	1 M H_2SO_4	CV (1 $mA \cdot cm^{-2}$)	909	–	[46] (2014)
Covalently-grafted on GO	3-electrode	1 M H_2SO_4	CV (1 $A \cdot g^{-1}$)	442	82% (2000 cycles)	[24] (2014)
One-step electrochemical codeposition GO-PANI	3-electrode	1 M H_2SO_4	CV ($v = 10v \cdot s^{-1}$)	1136.4	89% (1000 cycles)	[47] (2013)
Graphene-wrapped PANI nanowire arrays on nitrogen-doped carbon fabric	3-electrode	1 M H_2SO_4	CV (1 $A \cdot g^{-1}$)	1145	94% (5000 cycles)	[20] (2014)
Graphene-wrapped PANI with worm-like structures via a simple polymerization	3-electrode	1 M H_2SO_4	CV (0.5 $A \cdot g^{-1}$)	488.2	72.4% (1000 cycles)	[49] (2013)
Graphene-wrapped PANI with core–shell structures	3-electrode	1 M H_2SO_4	CV (1 $A \cdot g^{-1}$)	614	90% (500 cycles)	[50] (2013)
Graphene-wrapped PANI with film structures by LBL on Pt substrate	3-electrode	0.5 M H_2SO_4	CV (1 $A \cdot g^{-1}$)	1443	68% (500 cycles)	[44] (2013)
Graphene-wrapped PANI with film structures by LBL on ITO glass substrate	3-electrode	1 M H_2SO_4	CV (3 $A \cdot cm^{-3}$)	1562 $F \cdot cm^{-3}$	82% (1000 cycles)	[51] (2013)

SC electrodes. The authors attributed this to the synergistic effect between PANI and GO. They believed that they formed a uniform hierarchical morphology within PANI-GO thin films, and short rod-like nanostructures that had densely grown on the GO sheets.

The aforementioned graphene-PANI composites structures share a common feature of graphene surrounded by PANI. That is, graphene or GO was prepared first, and then PANI is anchored on the surface. Reverse structures have also been prepared in which PANI is surrounded by graphene. For instance, Yu et al. reported graphene-wrapped PANI nanowire arrays on nitrogen-doped carbon fabric for SCs. Firstly, conducting PANI nanowire arrays were deposited on a nitrogen-doped carbon fabric electrode. Then, a layer of rGO sheets was wrapped on PANI (Fig. 8).[20] Both specific capacitance and cycling stability of the prepared composites were higher than that without the graphene coating layer. In this configuration, the graphene coating layer was used to accommodate the volume change and mechanical deformation during the charge/discharge processes of the PANI-GO composites.

The graphene-wrapped PANI composites may feature different shapes, depending on the preparation methods, such as worm-like structures via a simple polymerization

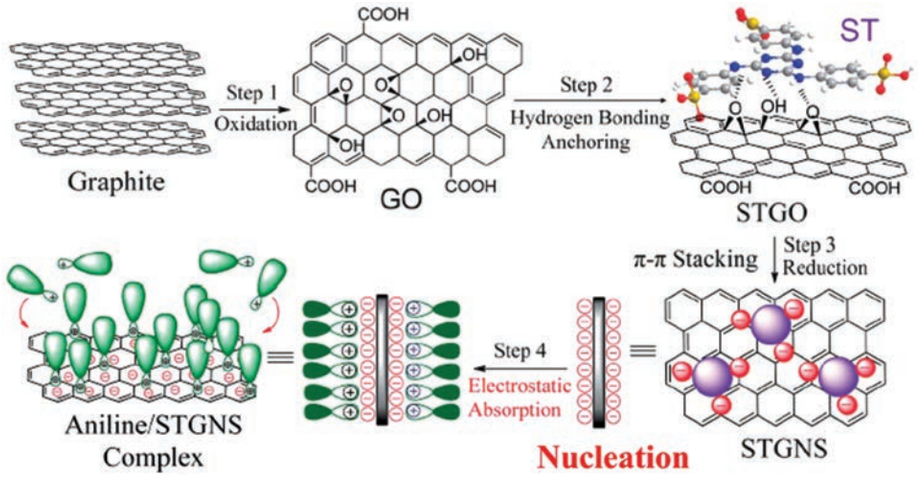

Fig. 6. Schematic representation of the fabrication of PANI–STGNS hybrids. Reproduced with permission from [44], L. Li, et al., *Nano Energy* 2, 628 **(2013)**. © 2013, Royal Society of Chemistry.

route,[49] core–shell structures by using micro-spherical sacrificed templates,[50] ultrathin film structures by using flat substrate and LBL assembly methods.[44,51] All these composites have magnificent electrochemical properties. Therefore, rational design and synthesis of graphene-PANI composite with controllable structures is particularly advantageous for SCs.

Additionally, PANI derivatives, e.g., poly(o-anisidine) (POA),[52] poly(o-toluidine) (POT),[53] poly(ortho-phenylenediamine) (PoPD) and poly(N-acetylaniline) (PAANI),[32,54] have also been developed and compounded with graphene for SCs. For instance, Punya et al. compared the electrochemical properties of graphene-based composites with PANI and derivatives.[53] They found that graphene-POT composites exhibited better capacitance (425 $F \cdot g^{-1}$) than graphene-PANI composites (400 $F \cdot g^{-1}$) due to the excellent electron donating properties of POT. They also found that graphene-POA composites possessed good electrochemical performance, because the presence of the electron-donating group ($eOCH_3$) in o-anisidine enhanced charge transport in the graphene-POA electrodes through the lone pair of nitrogen electrons.[52] Recently, Li et al. synthesized graphene-PAANI composites with ultrahigh specific capacitance (1126 $F \cdot g^{-1}$) by using the electropolymerization route.[54] The high specific capacitance paved the way for the fabrication of novel SCs (Table III, Fig. 9).

2.2. Graphene-Polypyrrole/Polythiophene Composites

Polypyrrole (PPy) and polythiophene (PTo) and their derivatives make up another class of CPs, which have also been used as promising pseudo-capacitive materials for SCs. However, the poor cycling stability greatly restricts their applications, similar to PANI. To overcome this shortcoming, the construction of graphene-PPy (or PTo) composites with ordered carrier passages has been proposed as a potentially admissible strategy.[55]

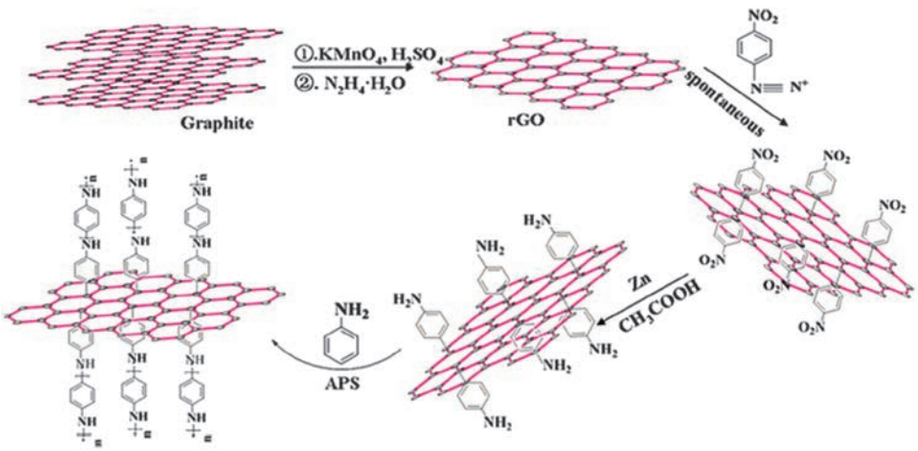

Fig. 7. Procedure for the fabrication of PANI-functionalized RGO. Reproduced with permission from [36], L. Wang, et al., *Sci. Rep.* 3, 3568 **(2013)**. © 2013, Rights Managed by Nature Publishing Group.

REVIEW

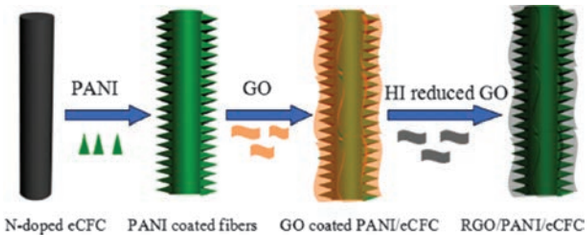

Fig. 8. Procedure to Coating RGO Nanosheets on PANI Nanowire Arrays Deposited on Nitrogen-Doped carbon fabric electrode. Reproduced with permission from [20], P. Yu, et al., *Langmuir* 30, 5306 **(2014)**. © 2014, American Chemical Society.

The methods to prepare graphene-PPy (or PTo) composites are about the same as those for graphene-PANI, including *in-situ* and *ex-situ* polymerization,[56, 57] electrochemical and chemical oxidative polymerization,[58, 59] etc. *Ex-situ* polymerization mainly refers to directly mixing the solutions of PPy with graphene, GO or rGO after they are prepared separately a prior. In another study, Qian et al. fabricated a rGO-PPy core–shell composite via electrostatic interactions and π–π stacking interactions.[56] Firstly, positively charged PPy microspheres were synthesized from pyrrole polymerization. Secondly, GO sheets with negatively charged groups were coated onto the PPy microspheres via electrostatic interactions and accumulation through π–π interactions; the product was then reduced by hydrazine. The composite exhibited a crumpled surface and a remarkable performance for SCs. The authors ascribed the improved capacitance to the high dispersibility, high conductivity and crumpled surface of the composite that diminished diffusion length (Fig. 10).

Compared to *ex-situ* polymerization, *in-situ* polymerization appears to exhibit further improvement. Gupta et al. compared graphene/poly(3-hexylthiophene) (P3HT) composites synthesized by *in-situ* and *ex-situ* polymerization. They found that *in-situ* P3HT formed better composites with rGO and exhibited higher specific capacitance and lower "IR drop" than the *ex-situ* sample (Fig. 11).[57] A possible explanation was that the combination between graphene and PCs via *in-situ* polymerization was much closer and more stable than the *ex-situ* counterpart.

In-situ polymerization typically includes two methods: polymerization of monomers in a suspension of graphene after reducing the GO, and polymerization of monomers in GO dispersions followed by reduction of GO. Studies suggest that the composites prepared by the former route is unfavorable for the construction of stable structures, because water-insoluble graphene is hard to disperse uniformly in aqueous solutions.[55] Therefore, the latter strategy is more vigorously explored where well-soluble GO is used instead of poorly-soluble graphene in aqueous solutions containing polymerizable monomers, followed by reducing the obtained GO/CP composites. For instance, Liu et al. synthesized rGO/PPy composites for SCs via *in situ* oxidation polymerization of pyrrole monomers in aqueous GO solutions, followed by chemical reduction of GO using ethylene glycol. The prepared composites showed highly enhanced conductivity and specific capacitance.[55] The authors attributed the excellent electrochemical capability to the high dispersibility and sound composite construction that improved the effective utilization of electroactive PPy components, accelerated shuttling charge carriers, and alleviated swelling/shrinkage of the polymer chains, because unlike the commonly employed hydrazine the moderate ethylene glycol reductant did not destruct the PPy conjugative structures (Table IV, Fig. 12).

3. GRAPHENE-TRANSITION METAL OXIDES/HYDROXIDES/SULFIDES COMPOSITES

In addition to CPs, transition-metal oxides (hydroxides or sulfides) (e.g., RuO_2, MnO_2, Co_3O_4, $Ni(OH)_2$, CoS, CuO, Fe_2O_3, ZnO, and so on.) are another type of active electrode materials for pseudo-capacitive SCs. However, their drawbacks, such as poor conductivity and low operating voltages seriously reduce the power density and energy density of SCs. Moreover, the tendency of aggregation and poor cycling capability has also limited their further applications. To address these issues, in combination with graphene, which is usually used as conductive additive and flexible substrates (or backbone materials), they can achieve ultrahigh values of capacitance for pseudo-capacitor electrodes.

The mechanism and effect of graphene-metal oxide composites is similar to that of graphene-CPs composites. Firstly, graphene provides large surfaces to anchor metal oxide particles;[63] secondly, graphene serves as a highly conductive matrix to support pathways for charge transport;[64] thirdly, metal oxides deposited on the graphene surface prevent the aggregation of graphene;[63] fourthly, graphene can restrict the mechanical deformation of the

Table III. Summary of SC performance of composites of graphene and PANI derivatives.

Electrode active materials	Electrode configuration	Electrolyte	Measurement protocol	Maximum capacitance ($F \cdot g^{-1}$)	Capacitance retention	Ref. (year)
Graphene-POA	3-electrode	2 M H_2SO_4	CV (1 $mA \cdot g^{-1}$)	380	73% (1000 cycles)	[52] (2013)
Graphene-POT	3-electrode	2 M H_2SO_4	CV (1 $mA \cdot g^{-1}$)	425	–	[53] (2013)
Graphene-PoPD	3-electrode	2 M H_2SO_4	CV (0.1 $A \cdot g^{-1}$)	308	99% (1500 cycles)	[32] (2013)
Graphene-PAANI	3-electrode	1 M H_2SO_4	CV (10 $mV \cdot s^{-1}$)	1126	94% (1000 cycles)	[54] (2014)

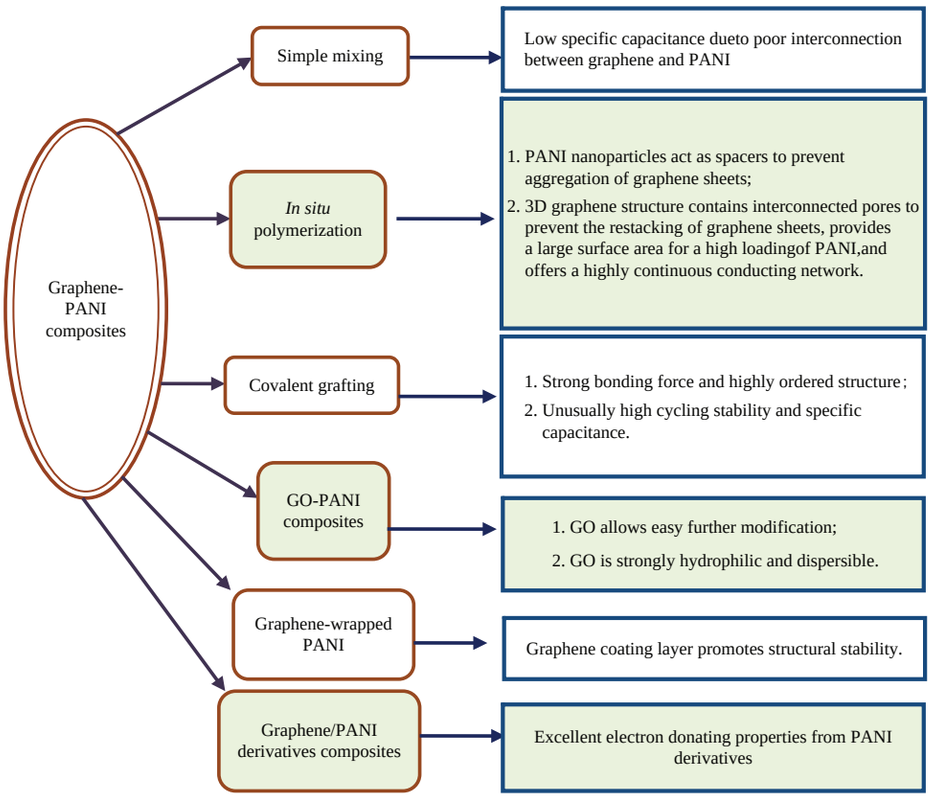

Fig. 9. Summary of graphene-PANI composites for SCs.

active components during charging–discharging process, thus leading to improved stability with its unique structural and mechanical properties.[65] Consequently, the composites of graphene-metal oxides not only combine the merits and mitigate the shortcomings of both components, but also realize the synergistic effects of pseudo-capacitive and EDLC performance.

3.1. Graphene/Mn-Based Composites

Among the various metal oxides used as pseudo-capacitors, RuO_2 stands out as the best performer.[66] However, due to high costs and environmental concerns,[67] RuO_2 has been replaced with other less expensive transition-metal oxides, such as Co_3O_4, $Co(OH)_2$, NiO, $Ni(OH)_2$, MnO_2, etc.[68–71] In fact, Mn-based (MnO_x) materials has been preferred due to its high theoretical capacitance (1370 $F \cdot g^{-1}$), variable oxidation states (MnO_2, Mn_2O_3 and Mn_3O_4), low costs, eco-friendly nature and high abundance.[27,72] Accordingly, great attempts have been made to prepare graphene/MnO_x nanocomposites for SCs by adopting different synthetic strategies.

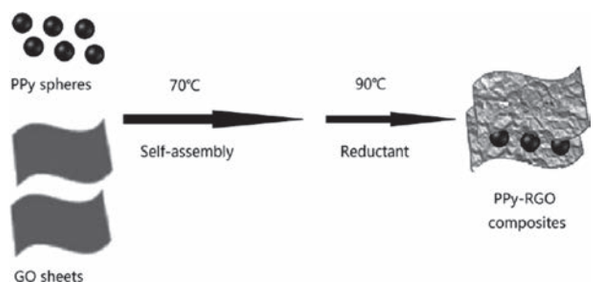

Fig. 10. Fabrication of PPy-rGO composites. Reproduced with permission from [56], T. Qian, et al., *J. Mater. Chem. A* 1, 6539 (**2013**). © 2013, Royal Society of Chemistry.

Generally, there are three types of reaction procedures to fabricate graphene-MnO_x nanocomposites.

(a) MnO_x is formed on GO using various functional groups, followed by reduction of graphene to rGO yielding rGO-MnO_x.[15,71]

(b) With an opposite reaction order, GO is reduced to rGO firstly, onto which MnO_x is formed.[64,73]

(c) MnO_x is formed on GO, and at the same time, GO is reduced to rGO simultaneously.

For instance, Subramani et al. prepared Mn_3O_4–rGO nanocomposites via the (a) procedure. Firstly, the Mn_3O_4 nanocubes were chemically decomposed on the GO nanosheet surface. Secondly, GO was reduced to rGO by hydrazine. The resulting composites exhibited enhanced electrochemical performances (Fig. 13).[71]

Liu et al.,[72] Ge et al.,[74] and Song et al.[64] respectively synthesized MnO_2-graphene hybrids via the (b) procedure. Firstly, graphene was prepared by chemical reduction of GO using hydrazine (or HI) or from the exfoliated GO by

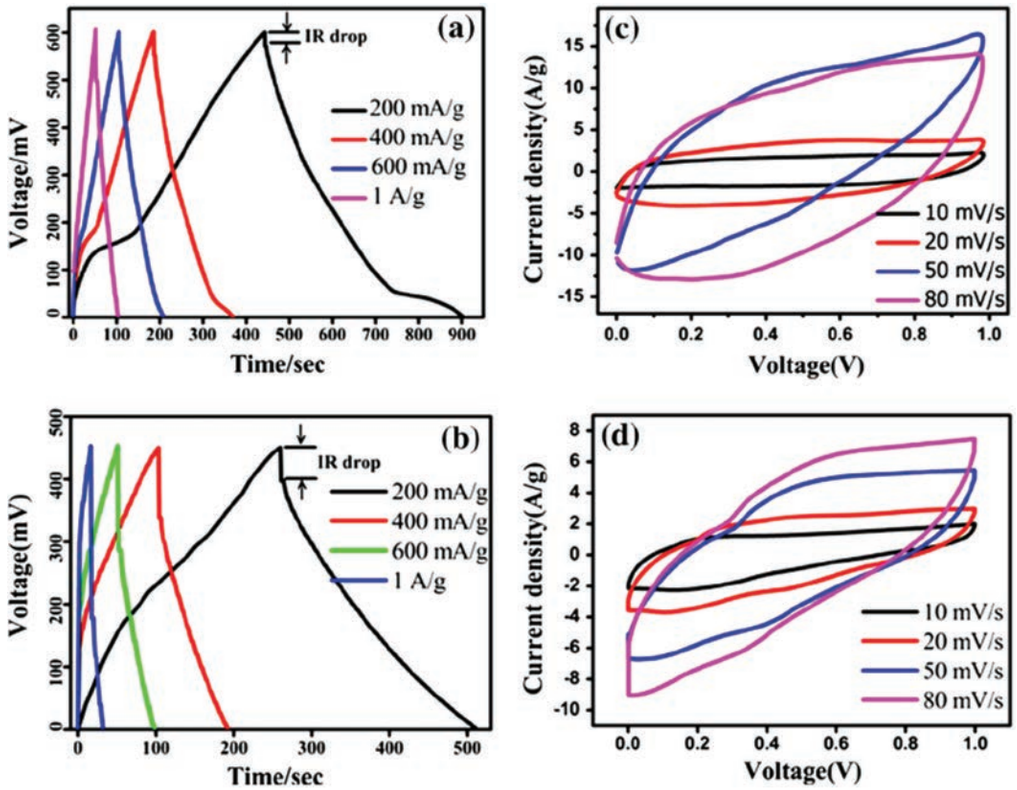

Fig. 11. Galvanostatic charging/discharging curves for (a) *in-situ* and (b) *ex-situ* rGO-P3HT composites and cyclic voltammograms (CV) for (c) *in-situ* and (d) *ex-situ* rGO-P3HT composites. Reproduced with permission from [57], A. Gupta, et al., *Mater. Chem. Phys.* 140, 616 **(2013)**. © 2013, Elsevier B.V.

microwave irradiation. Secondly, MnO_2-graphene hybrid was obtained by a hydrothermal treatment of the mixture of $KMnO_4$ and graphene. The composites exhibit excellent an electrochemical performance (Fig. 14).

A comparative study of the (a) and (b) procedures has been made by Kim et al. For the (a) strategy, the MnO_2 nanostructures were homogeneously dispersed on graphene sheets (S1 in Fig. 15), whereas MnO_2 nanostructures in (b) formed aggregates on graphene sheets (S2 in Fig. 15). The S1 composite electrode exhibited a higher specific capacitance than S2 (Fig. 15).[75] GO was highly dispersible in water due to oxygenated functional groups.[23] With the hydrophilic nature of GO, MnO_x associated strongly and evenly precipitated onto GO sheets in aqueous solutions. In contrast, in the (b) procedure, homogeneous dispersion of MnO_x nanostructures could not be formed because of the absence of functional groups on graphene sheets and their hydrophobic nature. Moreover, the oxygen-containing functionalities (epoxide, hydroxyl, carbonyl and carboxyl groups) of GO acted as anchor sites, enabling the subsequent *in situ* formation of MnO_x nanostructures that were attached to the surfaces of GO sheets.[76] Note that the attachment between graphene and MnO_x was based mainly on physical adsorption in (b). Therefore the (a) procedure is generally preferred than the (b) procedure.

There is another point that needs to be highlighted in the (a) procedure. That is, the GO must be reduced to rGO after MnO_x nanostructures are anchored because GO lacks electronically conductive channels.[77] So GO-MnO_x composites typically feature a much lower specific capacitance than rGO-MnO_x composites. Kim et al. studied the electrochemical performance of rGO/MnO_2 composites reduced by different chemical reduction methods. They found that the rGO/MnO_2 composites reduced by hydrazine hydrate (H-rGO/MnO_2) yielded a higher specific capacitance than that reduced by sodium borohydride (S-rGO/MnO_2), because H-rGO/MnO_2 was more effective in forming electronically conductive channels than S-rGO/MnO_2 with a lower concentration of oxygen-containing functional groups.[27]

However, an appropriate concentration of residual oxygen-containing functional groups on rGO–MnO_x composites is actually beneficial to the electrochemical performance. Kim et al. reduced graphene–MnO_2 composites by various concentrations of hydrazine hydrate with a fixed reduction time to control the concentration of the residual oxygen-containing functional groups, which was found to affect the electrical conductivity and density of

Table IV. Summary of SC performance of graphene/PPy or PTo composites.

Preparation method	Electrode configuration	Electrolyte	Measurement protocol	Maximum capacitance ($F \cdot g^{-1}$)	Capacitance retention	Ref. (year)
In-situ chemical grafting polymerization of pyrrole in the presence of modified graphene	3-electrode	1 M $NaNO_3$	CV (10 $mV \cdot s^{-1}$)	191.2	63% (1000 cycles)	[60] (2013)
In situ oxidation polymerization of pyrrole in GO solutions, followed by chemical reduction	3-electrode	1 M H_2SO_4	CV (0.5 $A \cdot g^{-1}$)	420	93% (200 cycles)	[55] (2013)
In-situ chemical polymerization of pyrrole in the presence of graphene	3-electrode	1 M KCl	CV (10 $mV \cdot s^{-1}$)	466	85% (600 cycles)	[58] (2013)
In-situ electrochemical polymerization of pyrrole in the presence of 3D graphene foam containing pyrrole	3-electrode	3 M $NaClO_4$	CV (1.5 $A \cdot g^{-1}$)	350	100% (1000 cycles)	[61] (2013)
Ex-situ PPy-rGO core–shell composite	3-electrode	1 M KCl	CV (0.5 $A \cdot g^{-1}$)	557	85% (1000 cycles)	[56] (2013)
In-situ electrodepostion of GO/PPy composite	3-electrode	1 M NaCl	CV (0.1 $V \cdot s^{-1}$)	960	–	[59] (2014)
Microwave-assisted *in situ* synthesis of graphene/PEDOT hybrid	3-electrode	1 M H_2SO_4	CV (1 $A \cdot g^{-1}$)	270	93% (10000 cycles)	[62] (2013)
Synthesized P_3HT/graphene composites via both *in-situ* and *ex-situ*	2-electrode	1 M H_2SO_4	CV (200 $mA \cdot g^{-1}$)	244 (*ex-situ*) 323 (*in-situ*)	–	[57] (2013)

the MnO_2 nanoneedles and hence the surface area and the SCs performance. They found that when rGO-MnO_2 was reduced by a high concentration of hydrazine (70%, denoted as rGO–MnO_2 (70)), the composite exhibited a low sheet resistance value but also a low surface area and pore volume. At a lower concentration of hydrazine (e.g., 50%, rGO-MnO_2 (50)), whereas a large amount of oxygen-containing functional groups on MnO_2 as well as hydroxyl, epoxy, and carboxylic groups on GO sheets were removed, the rGO–MnO_2 (50) composite remained high oxidized, leaving a high specific surface area and pore volume for ion adsorption and diffusion.[77]

The composition ratio between graphene and MnO_x,[78,79] the size, thickness, crystallographic forms (α, β, δ and γ) and morphologies (nanoneedles, nanowires, nanorods, nanoparticles, nanospheres, nanocubes, and nanospindles) of MnO_x also play a vital role in the determination of the SCs performances.[75,80] Mondal et al. fabricated graphene-MnO_2 hybrid nanosheets at different ratios. They found that the specific capacitance of the hybrids was strongly dependent on the graphene/MnO_2 ratio. At the graphene/MnO_2 ratio of 1:4, the hybrid electrode exhibited a high specific capacitance. Lower ratios of graphene nanosheets resulted in less space to anchor the MnO_2 nanosheets. Therefore, the utilization of the MnO_2 was lower, which resulted in a smaller specific capacitance and lower capacitance retention (Fig. 16).[78] In another study, Xiao et al. also found that when the graphene content was about 15.3 wt% (loading of Mn_3O_4 84.7%), the nanocomposites exhibited the maximal specific capacitance. With the poor conductivity of active Mn_3O_4, it is critical to adjust the ratio between Mn_3O_4 to graphene to optimize the electron transport and ion diffusion of the nanocomposites.[79] It is known that only the surface (or a very thin surface layer of the oxide) of MnO_x can participate in pseudo-capacitive reactions. Therefore, the specific capacitance decreases with increasing thickness of MnO_x because of low utilization of the total MnO_x as well as poor electrical conductivity of the MnO_x.[27]

With respect to crystallographic forms and morphologies, researchers have found that MnO_2 with α

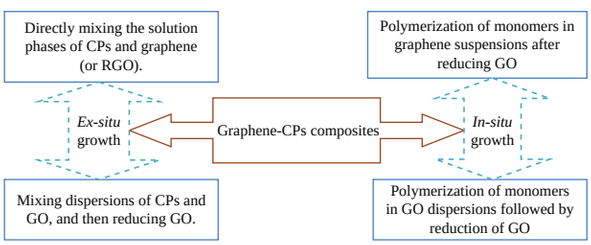

Fig. 12. Summary of SCs based on graphene-CP composites.

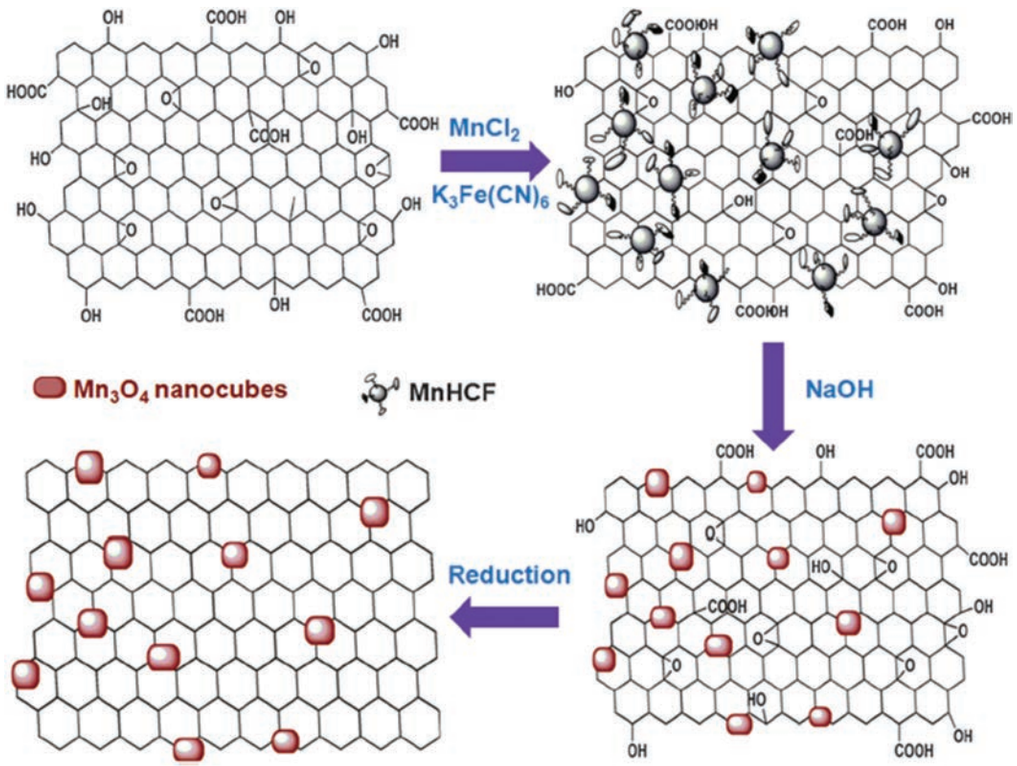

Fig. 13. Preparation of Mn_3O_4–RGO nanocomposites. Reproduced with permission from [71], K. Subramani, et al., *Phys. Chem. Chem. Phys.* 16, 4952 **(2014)**. © 2014, Royal Society of Chemistry.

crystallographic structures exhibited the optimal specific capacitance.[75, 80] Also it has been found that needle-like MnO_2 exhibited a higher specific capacitance than other forms,[75, 80] likely because a 1D structure like nanowires and nanoneedles can effectively create interconnections between metal oxides and graphene. For example, Kim et al. found that the composites of graphene and MnO_2 nanoneedles showed an excellent SC performance.[80] Wang et al. found that the specific capacitance of graphene-MnO_2 nanowire composites was higher than that of composites based on graphene-MnO_2 nanoparticles.[81] In addition, Feng et al. demonstrated that graphene-MnO_2 composite with MnO_2 showing a flower-like structure exhibited a capacitance of 405 $F \cdot g^{-1}$, markedly better than other graphene-MnO_2 composites with a nanowire morphology at 318 $F \cdot g^{-1}$.[82] One possible reason is that flower-like nanospheres possessed a larger specific surface area than nanowires.

Note that the specific surface area of the active materials is critical to the electrochemical performance of SCs. Thus, a number of effective strategies have been developed to prepare graphene-MnO_x composites based on, for instance, supercritical CO_2 ($SCCO_2$),[83] 3D networks hydrogel,[84, 85] aerogels,[86] and porous flexible template methods.[87] For instance, Lee et al. reported that $SCCO_2$ was ideal for synthesizing nanomaterials and uniformly dispersing them onto a high-surface-area supporting material. MnO_2 nanorods prepared by $SCCO_2$ showed an extremely high surface area. Furthermore, $SCCO_2$ could help debundle the graphene nanosheets and uniformly disperse the MnO_2 nanorods, thus preventing graphene restacking and obtaining high electrochemical utilization. As expected the $SCCO_2$-MnO_2/graphene showed superior SCs properties.[83]

It is well known that graphene can be used as building blocks for the self-assembly into 3D hydrogel or

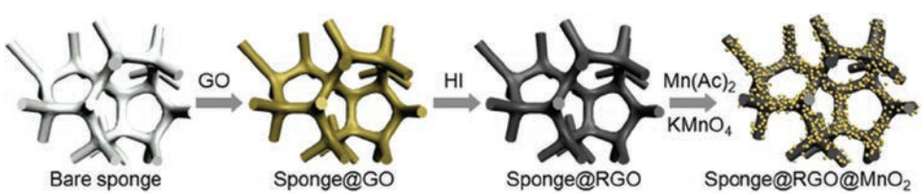

Fig. 14. Schematic illustration of the preparation of rGO-MnO_2 composites by a dip coating process. Reproduced with permission from [74], J. Ge, et al., *Nano Energy* 2, 505 **(2013)**. © 2013, Elsevier Ltd.

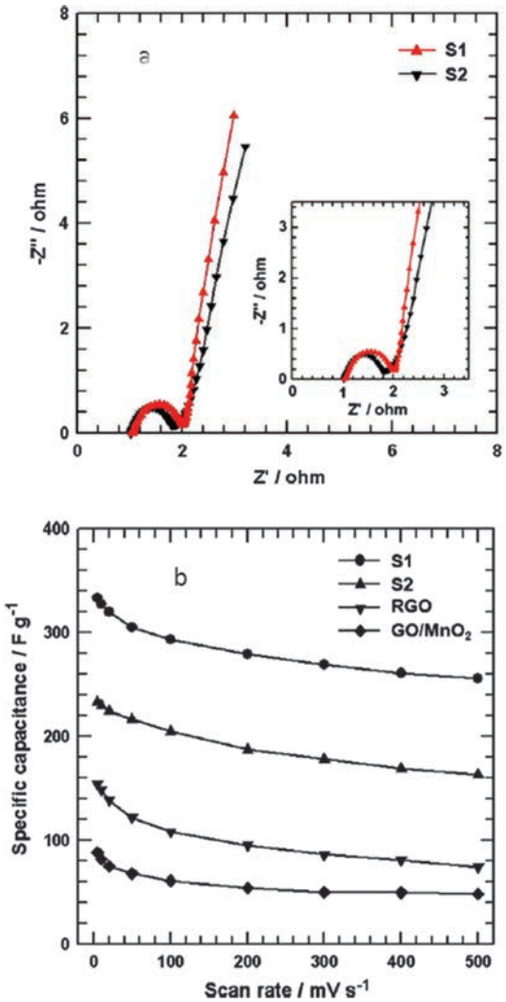

Fig. 15. (a) Nyquist plots of S1 and S2. (b) Specific capacitance of S1 and S2 at different scan rates. Reproduced with permission from [75], M. Kim, et al., *Chem. Eng. J.* 230, 482 **(2013)**. © 2013, Elsevier B.V., All rights reserved.

aerogel structures. It has been reported that assembling graphene nanosheets into hydrogel or aerogel with a 3D interconnected microporous and mesoporous networked structure could effectively prevent the aggregation of graphene nanosheets. Consequently, the hydrogel or aerogel may be used as potential SC electrode materials due to their large active surface areas and convenient electrolyte ion transport. Accordingly these materials demonstrate an enhanced energy storage capacity and a good rate capability.[84–86] For instance, Wu et al. fabricated 3D networks of graphene-MnO_2 hydrogel via *in situ* self-assembly. First, MnO_2 nanoparticles were grown onto the surfaces of GO nanosheets. Then the rGO-MnO_2 composite hydrogel was prepared by reduction-induced *in situ* self-assembly. The prepared 3D graphene-MnO_2 hydrogel showed a high performance for SC applications and it could be used directly as electrodes without any other polymer binders or conducting additives (Fig. 17).[85]

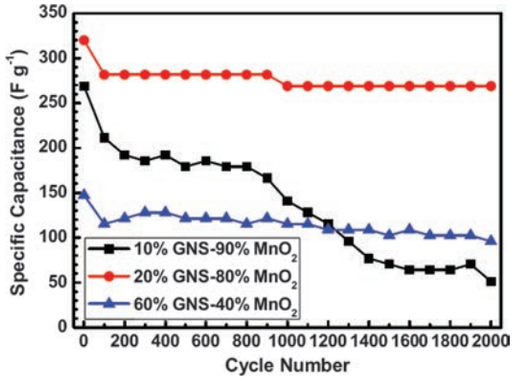

Fig. 16. Comparison of the cycling performance of graphene/MnO_2 hybrid nanosheets at different ratios in 1 M Na_2SO_4 at the current density of 500 $mA \cdot g^{-1}$ (GNS is graphene nanosheets). Reproduced with permission from [80], M. Kim, et al., *J. Mater. Sci.* 48, 7652 **(2013)**. © 2014, Elsevier B.V.

Li et al. synthesized 3D networks of a Mn_3O_4-rGO hydrogel by a hydrothermal self-assembly route. The obtained Mn_3O_4-rGO hydrogel exhibited excellent cycling stability and rate capability.[84]

Wang et al. prepared MnO_2-graphene aerogel composites by a two-step method.[86] Firstly, graphene aerogels were prepared through sol–gel chemistry. Secondly, The MnO_2 was electrochemically deposited into the highly porous graphene aerogel to form MnO_2-graphene aerogel composites. When the mass loading of MnO_2 was 61 wt%, the aerogel exhibited the maximum specific capacitance. The authors attributed the high performance to the structural advantages of high specific surface areas, high pore volumes, large pore sizes, and a 3D well-connected network of the graphene aerogel support. Moreover, with the sol–gel polymerization, chemical linkages were formed at the graphene sheet junctions, so the graphene aerogels possessed high electrical conductivity and low charge-transport resistance.

A 3D porous flexible template not only provides a porous scaffold, but also acts as a light weight, flexible electrode. Flexible and lightweight SCs have attracted great attention due to increasing energy demand for portable and wearable electronics.[87] Generally, to make flexible SCs, flexible and binder-free electrodes with favorable mechanical strength and large capacitance are required. Some flexible conductive templates have been chosen as substrates for flexible electrodes, such as carbon fabric cloth, carbon fiber paper, sponges and Ni foam.[88, 89] For instance, Ye et al. developed a flexible MnO_2–rGO electrode using carbon cloth as a substrate by a one-step electrochemical deposition method. The results demonstrated that the device possesed excellent mechanical flexibility and the electrochemical properties showed no obvious change even under bending and twisting.[88]

More advantages are anticipated for flexible and freestanding graphene-based paper electrodes than for

REVIEW

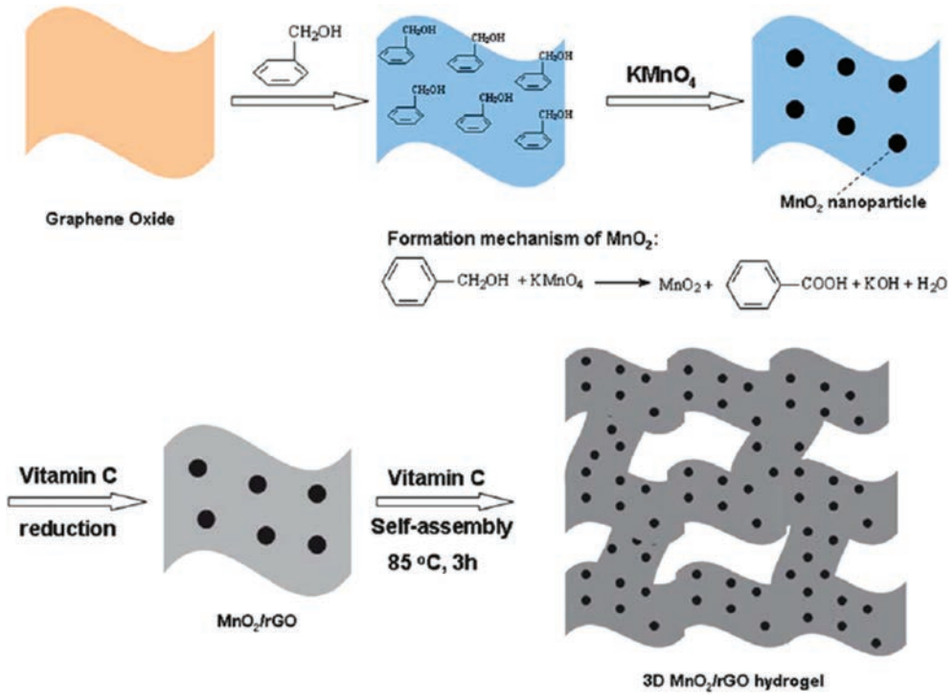

Fig. 17. Illustration of the formation of MnO_2 nanoparticles on the surface of GO, and subsequent reduction and *in situ* self-assembly of 3D MnO_2/RGO hydrogel. Reproduced with permission from [87], Y. He, et al., *Acs Nano* 7, 174 (**2013**). © 2013, Royal Society of Chemistry.

template electrodes. Peng et al. reported a novel, high-performance in-plane SCs based on MnO_2/graphene nanosheet hybrids.[90] The high malleability of the planar SCs makes led to superior flexibility and robust cyclability, and the device yielded a capacitance retention over 90% after 1000 times of folding/unfolding.

In summary, with proper design and preparation, the structure and size of the composites may be controlled at

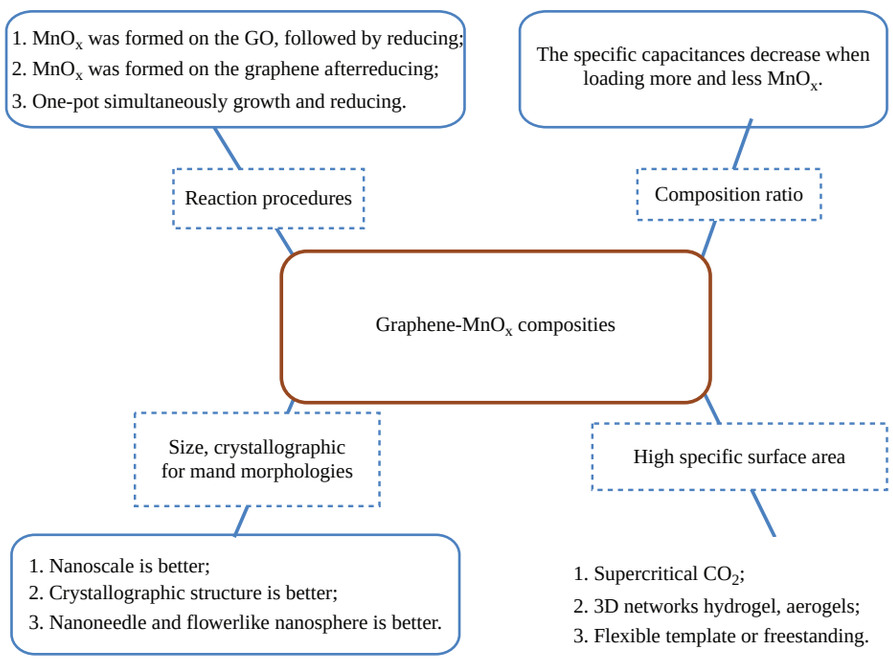

Fig. 18. Summary of SC performance of graphene-MnO_x composites.

Table V. Summary of SC performance of graphene-MnO_x composites.

Preparation method or active material of electrode	Electrode configuration	Electrolyte	Measurement protocol	Maximum capacitance ($F \cdot g^{-1}$)	Capacitance retention	Ref. (year)
In-situ growth of MnO_2 nanowires on graphene after exfoliated GO by microwave irradiation	3-electrode	1 M Na_2SO_4	CV (0.5 $A \cdot g^{-1}$)	276	100% (1200 cycles)	[64] (2014)
MnC_2O_4-graphene composites, prepared by a hydrothermal process after exfoliated GO by microwave irradiation	3-electrode	6 M KOH	CV (0.5 $A \cdot g^{-1}$)	122	94.3% (1000 cycles)	[72] (2013)
MnO_2-graphene hybrid, prepared by a hydrothermal process after reduction by hydrazine	3-electrode	1 M Na_2SO_4	CV (0.2 $A \cdot g^{-1}$)	315	87% (2000 cycles)	[73] (2013)
Chemical decomposition Mn_3O_4 nanocubes on GO followed by reduction with hydrazine	3-electrode	1 M Na_2SO_4	CV (0.5 $A \cdot g^{-1}$)	131	99% (500 cycles)	[71] (2014)
Graphene–MnO_2 composites reduced from GO–MnO_2 with hydrazine	3-electrode	1 M Na_2SO_4	CV (10 $mV \cdot S^{-1}$)	383.82	85.1% (1000 cycles)	[77] (2013)
Graphene/MnO_2 composites reduced from GO–MnO_2 with hydrazine (S1)	3-electrode	1 M Na_2SO_4	CV (10 $mV \cdot S^{-1}$)	327.5	90% (1000 cycles)	[75] (2013)
Graphene/MnO_2 composites prepared after reduction with hydrazine (S2)	3-electrode	1 M Na_2SO_4	CV (10 $mV \cdot S^{-1}$)	229.9	90% (1000 cycles)	[75] (2013)
MnO_2-GO hybrid by hydrothermal method	3-electrode	1 M Na_2SO_4	CV (0.1 $A \cdot g^{-1}$)	213	98.1% (1000 cycles)	[76] (2013)
One-pot hydrothermal synthesis of Mn_3O_4/graphene	3-electrode	1 M Na_2SO_4	CV (1 $A \cdot g^{-1}$)	171	93% (50 cycles)	[91] (2013)
Graphene/MnO_2 hybrid with a weight ratio of 1:4	3-electrode	1 M Na_2SO_4	CV (0.5 $A \cdot g^{-1}$)	320	87.5% (2000 cycles)	[78] (2014)
Graphene-Mn_3O_4 composites with a weight ratio of 15.3:84.7	3-electrode	1 M Na_2SO_4	CV (1 $A \cdot g^{-1}$)	239	107% (1000 cycles)	[79] (2014)
Nanoneedle structure of MnO_2/graphene composites	3-electrode	1 M Na_2SO_4	CV (10 $mV \cdot S^{-1}$)	327.5	88.21% (1000 cycles)	[80] (2013)
Graphene–MnO_2 (flowerlike nanospheres)	3-electrode	1 M Na_2SO_4	CV (1 $A \cdot g^{-1}$)	405	90% (1000 cycles)	[82] (2014)
$SCCO_2$-MnO_2/graphene	3-electrode	3 M KCl	CV (50 $mV \cdot S^{-1}$)	230	98% (10000 cycles)	[83] (2013)
3D networks graphene-Mn_3O_4 hydrogel hydrothermal self-assembly	3-electrode	1 M Na_2SO_4	CV (1 $A \cdot g^{-1}$)	148	100% (1200 cycles)	[84] (2013)
3D networks graphene-MnO_2 hydrogel via *in situ* self-assembly	2-electrode	1 M Na_2SO_4	CV (1 $A \cdot g^{-1}$)	137	89.6% (1000 cycles)	[85] (2013)
MnO_2-graphene aerogels through sol–gel chemistry and electrochemical deposition process	3-electrode	0.5 M Na_2SO_4	CV (2 $mV \cdot S^{-1}$)	410	95% (50000 cycles)	[86] (2014)
Flexible MnO_2–RGO electrode using carbon cloth as substrate	2-electrode	Solid-state H_3PO_4/PVA	CV (2 $mV \cdot S^{-1}$)	14 $F \cdot cm^{-2}$	100% (5000 cycles)	[88] (2013)
Flexible and freestanding in-plane SCs based on MnO_2/graphene	2-electrode	PVA/H_3PO_4 gel	CV (0.2 $A \cdot g^{-1}$)	267	92% (7000 cycles)	[90] (2013)

the nanoscale, such that the electrochemical performance of graphene-MnO_x composites can be tuned even further (Fig. 18). Yet from Table V, we can see that the specific capacitance of graphene-MnO_x composites is still very low, usually 100 to 400 $F \cdot g^{-1}$. Further engineering of the electrode materials is desired.

3.2. Graphene/Ni-Based (Co-Based or Other Metal Oxides) Composites

Other novel electrode materials with high capacitance have also been explored for SCs. These include Ni-based materials (such as NiO, $Ni(OH)_2$, Ni_3S_2),[92–94] Co-based materials (such as CoO, Co_3O_4, CoS, Co_9S_8, $Co(OH)_2$, $CoFe_2O_4$, $CoMoO_4$),[26, 95–98] and other metal oxides materials (such as CuO, Fe_2O_3, Fe_3O_4, SnO_2, V_2O_5, WO_3, ZnO, etcetera).[99–105] The electrochemical performances of these metal oxides are similar to that of MnO_x. The preparation methods are also similar, including one-pot hydrothermal or solvothermal process,[106] hydrogel,[69] and 3D templates technique.[26, 107, 108]

Generally, graphene/metal-based composites are synthesized by one-pot hydrothermal or solvothermal process with GO and metal ion precursors as the starting materials. The metal ions are adsorbed on GO by electrostatic interactions where the oxygenated groups of GO sheets provide active sites for anchoring the metal ions.[109] During the hydrothermal (solvothermal) process, GO is reduced into rGO, and the metal-based active nanomaterials are formed and simultaneously grown *in situ* on the graphene sheets.[106] The metal-based nanoparticles may also be used as a spacer to prevent the graphene nanosheets from aggregating, and to stabilize the structure of the as-prepared graphene.[94] For instance, Xia et al. prepared $CoMoO_4$/graphene composites via a one-step hydrothermal method. The Co^{2+} ions were adsorbed on GO by electrostatic interactions and $CoMoO_4$ nanoparticles were grown on the graphene sheet after a hydrothermal reaction. The obtained composites exhibited low electrochemical resistance, good rate capabilities and excellent cycle life (Fig. 19).[106] Wu et al. prepared a homogenous $Ni(OH)_2$/graphene composite by an electrostatically induced stretch growth method, where the electrostatic interactions triggered advantageous changes in morphology and the ordered stacking of $Ni(OH)_2$ nanosheets on graphene also enhanced the crystallization of $Ni(OH)_2$ (Fig. 20).[109]

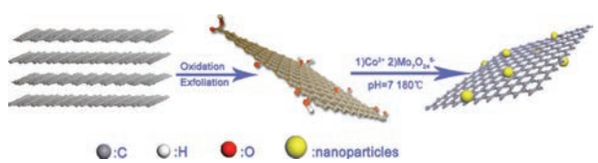

Fig. 19. Schematic illustration of the preparation of $CoMoO_4$/G. Reproduced with permission from [107], F. Zhang, et al., *Phys. Chem. Chem. Phys.* 16, 4186 **(2014)**. © 2013, Elsevier Ltd.

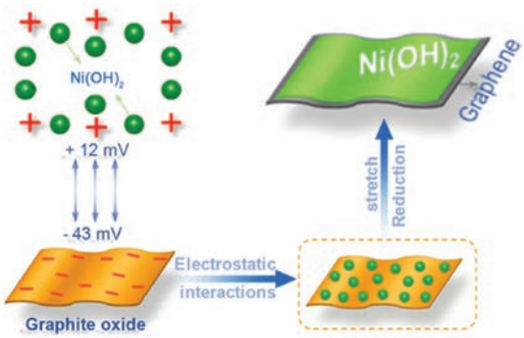

Fig. 20. Schematic illustration of $Ni(OH)_2$ stretch growth on graphene. Reproduced with permission from [108], C. Jiang, et al., *RSC Adv.* 4, 18080 **(2014)**. © 2014, Rights Managed by Nature Publishing Group.

Additionally, when other spacers are added in the aqueous solution containing GO and metal ion precursors during the synthesis process, they may effectively promote the formation of a high specific surface area. Zhang et al. synthesized bacteria promoted rGO-Ni_2S_3 (BGNS) networks using Bacillus subtilis as spacers. Compared with stacked rGO-Ni_2S_3 prepared without the aid of bacteria, BGNS showed a unique nm-μm structure which exhibited a higher specific capacitance than that of unaided synthesis.[110] Zhou et al. prepared a graphene-NiO composite assisted by glucose via a hydrothermal method. The glucose not only acted as a green reducing agent to produce rGO, but also transformed into a kind of amorphous carbon which, as a spacer, stabilized the structure of the as-prepared graphene. The obtained layered sandwich nanostructure exhibited a high specific capacitance.[94]

Generally, when Ni foams have been used as templates for preparing 3D graphene-based composites, the substrates need to be dissolved,[26, 107, 108] which not only produces a large amount of waste, but also complicates the process. Indirectly using 3D Ni foams coated with graphene-based composites as an electrode for SCs, without the need of any other binder materials and conductive agents, is very important and interesting for industrial production and study. Because Ni foams have high mechanical stability and an inherently continuous conductive network they can also act as current collectors.[111] Moreover, binder materials and conductive agents may also cause non-uniform distribution of the active materials and increase the charge-transfer resistance, both of which would significantly influence the performance of SCs.[92] For instance, Wang et al. reported a $Ni(OH)_2$/graphene/Ni foam electrodes fabricated by electrochemical deposition of $Ni(OH)_2$ nanoflakes on a graphene network grown on a Ni foam current collector.[92] The resulting binder-free $Ni(OH)_2$/graphene/Ni foam electrode exhibited an excellent SC performance. The authors ascribed the superior performances to the presence of a highly conductive graphene layer on the nickel foam, which they said

remarkably boosted the charge transfer process at the electrolyte/electrode interface. The 3D electrode formed by graphene/Ni foam was noted to dramatically lengthen the electrochemical cycling stability of the electrodeposited $Ni(OH)_2$ film and nanoflakes.

Zhang et al. presented a 3D Ni foam/graphene/Co_3S_4 composite film (Ni/G/CS) and used it as an SC electrode, which demonstrated a remarkable performance.[111] The authors attributed this to the formation of hollow nanospheres of a large specific surface area, extraordinary electrical conductivity, extremely high chemical stability of the graphene and high mechanical stability of Ni foam.

However, the electrodes by 3D Ni foam coated with graphene-based composites can not be used for flexible lightweight SCs because of the weight and thickness of nickel. Completely etching away the Ni foam may be on option; however, if the nickel foam is totally removed, the 3D graphene-based composite will lack structural support and likely exhibit poor SC performance as a result of reduced mechanical stability and increasing contact resistance. Recently, Huang et al. reported a simple strategy to obtain a flexible electrode by etching most of the Ni foam but maintaining the conductive backbone from the Ni foam.[112] This strategy greatly reduced the total mass of the electrode and provided a new direction for the development of flexible SCs.

When graphene-based composites are prepared by *in situ* growth of active materials directly on graphene, it may have resulted in inhomogeneous distribution. This difficulty of distribution may be due to the hydrophobicity of graphene which strongly resists crystal growth on its surface. To overcome this limitation some surfactants have been employed, such as sodium dodecyl benzene sulfonate (SDBS), ethanol, cetyltrimethylammonium bromide (CTAB) and polyvinylpyrrolidone (PVP),[97, 98, 108] to enhance uniform growth of active materials on the graphene surfaces where the morphologies may be manipulated by the choice of the surfactants. For instance, Jiang et al. synthesized 3D self-standing graphene/$Ni(OH)_2$ composites of different morphologies with SDBS and ethanol as surface active agents.[108] When SDBS was used to reduce the graphene hydrophobicity, $Ni(OH)_2$ was observed to have a uniform nanoflower morphology and formed a highly ordered film attached to the graphene surface. While an ethanol solution of 30% SDBS was used, the resulting $Ni(OH)_2$ showed a uniform nanosheet-like morphology on the graphene surface; whereas inhomogeneous distribution of $Ni(OH)_2$ particles was observed when they were grown without the addition of a surfactant solution. The 3D graphene/$Ni(OH)_2$ nanoflower composite was observed to have low resistance and good cycling performance, as compared to other morphologies. In another study, Ramachandran et al. prepared Co_9S_8, CoS, CoS/graphene nanocomposites in the presence of PVP, and the composites exhibited excellent electrochemical performance for SCs (Fig. 21) (Table VI, Fig. 22).[96, 97]

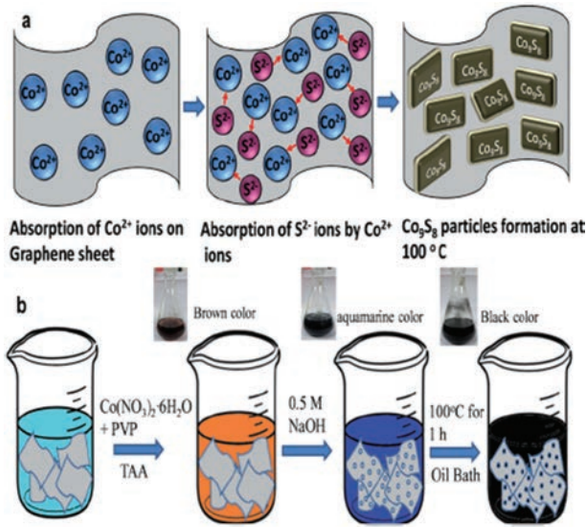

Fig. 21. (a) Schematic diagram and (b) experimental procedure of the formation of Co_9S_8/graphene nanocomposites, along with experimental photographic images. Reproduced with permission from [98], D. Ghosh, et al., *ACS Sustainable Chem. Eng.* 1, 1135 **(2013)**. © 2014, Royal Society of Chemistry.

3.3. Graphene-Binary Metal Oxides/Hydroxides

Binary metal oxide nanocomposites have attracted extensive attention because of their markedly better SC performance than that of single metal materials,[113] which may be ascribed to more facile electron transfer reactions. Mixed metal oxides exhibit higher electrical conductivity comparing to the pure metal oxides, and offer richer redox reactions than those of single metal oxides with contributions from both metal ions.[114] Of these, composites based on Ni–Co oxides,[114] Mn–Ni oxides,[115] Mn–Co oxides,[21] and Ni–Al oxides,[116] have attracted much interest in recent years. For instance, He et al. prepared $NiCo_2O_4$-rGO composites by a hydrothermal method. The solid-state redox couples of $Co^{2+}/Co^{3+}$and Ni^{2+}/Ni^{3+} presented in the structure provided a better electro-catalytic activity than those of NiO and Co_3O_4, a unique property for SCs.[113] Hwang et al. synthesized graphene/NiO–MnO_2 nanocomposites by chemical precipitation using a chelating agent along with Ni and Mn hydroxides on graphene.[115] Ghosh et al. synthesized α $MnMoO_4$-graphene hybrid via a hydrothermal procedure. The prepared materials responded in a wide range of working potentials. Synergy between graphene and pseudo-capacitive $MnMoO_4$ resulted in an increase of cycling stability and capacitance.[21]

Recently, layered double hydroxides (LDH) have also drawn enormous attention as an electrode material for SCs due to their abundant surface area and electrochemically active sites, which generate both electrical double-layer capacitance and pseudo-capacitance. LDH are a class of lamellar compounds that consist of positively charged brucite-like host layers, with a general chemical formula of $[M^{II}_{1-x}M^{III}_x(OH)_2]^{x+}[A^{n-}]_{x/n}$ mH_2O, where

Table VI. Summary of SC performance for graphene/Ni or Co-based composites.

Preparation method or active material of electrode	Electrode configuration	Electrolyte	Measurement protocol	Maximum capacitance ($F \cdot g^{-1}$)	Capacitance retention	Ref. (year)
In-plane and out-of-plane pores into a graphene–$Ni(OH)_2$ hybrid hydrogel	3-electrode	1 M KOH	CV (10 $mV \cdot s^{-1}$)	3138.5	95% (1000 cycles)	[69] (2013)
$Ni(OH)_2$-graphene by electrostatically induced stretch growth method	3-electrode	6 M KOH	CV (2 $mV \cdot s^{-1}$)	1503	96.5% (6000 cycles)	[109] (2014)
Bacteria promoted rGO-Ni_2S_3 using Bacillus subtilis as spacers	3-electrode	2 M KOH	CV (0.75 $A \cdot g^{-1}$)	1424	89.6% (3000 cycles)	[110] (2013)
Graphene-NiO composite assisted by glucose via hydrothermal method	3-electrode	6 M KOH	CV (0.5 $A \cdot g^{-1}$)	1495	90% (1000 cycles)	[94] (2014)
$Ni(OH)_2$/graphene/Ni foam by CVD and electrochemical depositing	3-electrode	1 M KOH	CV (3 $A \cdot g^{-1}$)	2161	63% (500 cycles)	[92] (2014)
3Dα-$Ni(OH)_2$-porous graphene hollow sphere use SiO_2 as template followed by etching with HF	3-electrode	2 M KOH	CV (5 $mV \cdot s^{-1}$)	2815	92.5% (1000 cycles)	[107] (2014)
3D Ni$(OH)_2$-graphene use Ni foam as template followed by Etching with HCl	3-electrode	6 M KOH	CV (6.7 $A \cdot g^{-1}$)	718.2	84.2% (500 cycles)	[108] (2014)
One-pot electrochemical co-deposition of Ni_2S_3/electrochemically reduced GO on Ni foam	3-electrode	1 M KOH	CV (2 $A \cdot g^{-1}$)	1392.2	66.8% (500 cycles)	[65] (2014)
CTAB-assisted βCo$(OH)_2$–graphene	3-electrode	6 M KOH	CV (2 $A \cdot g^{-1}$)	532	94% (500 cycles)	[98] (2013)
$CoMoO_4$/graphene composites via one-step hydrothermal method	3-electrode	6 M KOH	CV (1 $A \cdot g^{-1}$)	394.5	78.4% (500 cycles)	[106] (2013)
Co_3O_4/graphene composites via one-step hydrothermal method.	2-electrode	2 M KOH	CV (0.2 $A \cdot g^{-1}$)	263	92.09% (1000 cycles)	[95] (2013)
3D Ni foam/graphene/Co_3S_4 composite film	3-electrode	2 M KOH	CV (7.5 m $A \cdot cm^{-2}$)	0.525 ($F \cdot cm^{-2}$)	97.8% (8000 cycles)	[111] (2014)
Co9S8/graphene nanocomposites in the presence of PVP as surfactant	3-electrode	6 M KOH	CV (5 $mV \cdot s^{1}$)	808	99.2% (1000 cycles)	[97] (2014)
CoS/graphene nanocomposites in the presence of PVP as surfactant	3-electrode	6 M KOH	CV (5 $mV \cdot s^{1}$)	2423.3	–	[96] (2013)

M^{II} and M^{III} are mixed divalent and trivalent cations and A^{n-} can be almost any organic or inorganic anion. The graphene/LDH composites are promising electrode materials for SCs, in which the LDH sheets are effectively delaminated by the graphene sheets and the graphene sheets provide the resultant graphene/LDH composite with good electrical conductivity.[116–118] For instance, Memon et al. prepared composites of graphene and layered nickel and aluminum double hydroxides, and found that the crystallization behaviors and the morphology of the resulting LDH nanoparticles might be tuned by varying the GO and urea ratio. The obtained graphene/Ni–Al LDH nanowires exhibited multi-crystal features and represented a new assembly form of LDH materials. It showed enhanced performance for SCs compared with other morphologies of the Ni–Al LDH materials (Fig. 23). Xu et al.

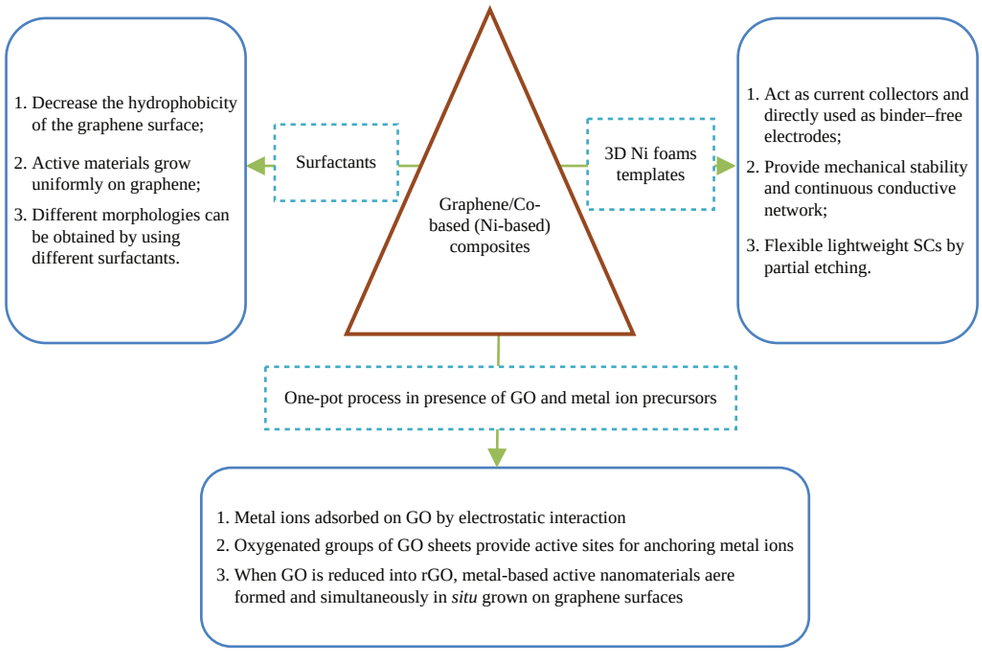

Fig. 22. Summary of SC performance for graphene/Co or Ni-based composites.

fabricated a hierarchical 3D graphene-LDH composite via a hydrothermal process. First, AlOOH colloids were coated on the graphene surfaces, then layered NiAl-LDH nanosheet arrays were *in situ* grown on the surfaces of graphene sheets forming a sandwich-like structure.[116] The composite exhibited a high specific capacitance because of its typical mesoporous structure with a large specific surface area.

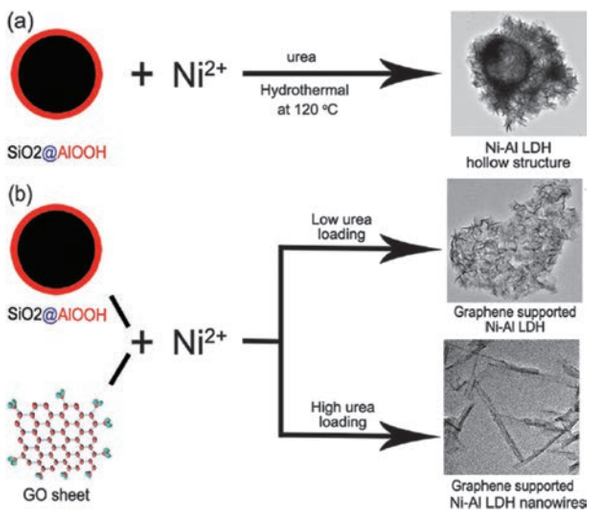

Fig. 23. Schematic illustration for the synthesis of graphene/Ni–Al LDH composites: (a) hollow spherical structures of Ni–Al LDHs synthesized in the absence of GO, (b) graphene supported Ni–Al LDH sheets and graphene/Ni–Al LDH nanowires synthesized in the presence of GO. Reproduced with permission from [118], G. Abellán, et al., *Part. Part. Sys. Char.* 30, 853 (**2013**). © 2014, Royal Society of Chemistry.

It has been reported that controlling the chemical composition in LDH materials is of utmost importance for SC applications. All LDH based nanocomposites generally lead to the formation of mixed metal oxides. Abellán et al. prepared $FeNi_3$ nanoparticles embedded in graphene by thermal decomposition of the $Ni^{II}Fe^{III}$-LDH precursor, which acted as a multilayered nanoreactor enabling the formation of a range of carbon nanoforms (CNFs). Different CNFs can be isolated by acid treatment of the as-prepared nanocomposites at different temperatures. These metal-carbon hybrids exhibited high values of specific capacitance and excellent rate capabilities (Fig. 24, Table VII).[118]

4. GRAPHENE-HETEROATOM COMPOSITES

Chemical doping of graphene with heteroatoms such as N, B, S and O is another effective approach to modulate its intrinsic electrical properties and thus

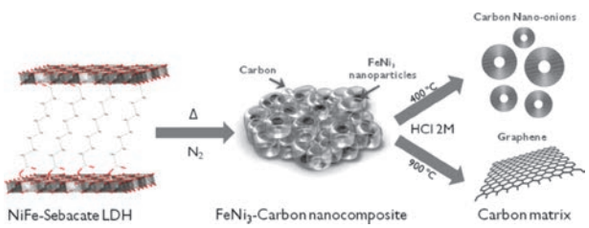

Fig. 24. Schematic illustration of the formation of $FeNi_3$–carbon nanocomposites and the corresponding CNFs obtained after the acid leaching procedure, i.e., carbon nano-onions at 400 °C and graphene at 900 °C. Reproduced with permission from [119], L. Wang, et al., *Electrochim. Acta* 111, 937 (**2013**). © 2013, Wiley-VCH.

Table VII. Summary of SC performance for graphene/binary metal oxides composites.

Preparation method or active material of electrode	Electrode configuration	Electrolyte	Measurement protocol	Maximum capacitance ($F \cdot g^{-1}$)	Capacitance retention	Ref. (year)
$NiCo_2O_4$-rGO by hydrothermal method	3-electrode	2 M KOH	CV (10 $mV \cdot s^{-1}$)	737	94% (3000 cycles)	[113] (2013)
$NiCo_2O_4$-rGO nanocomposite supported on Ni foam	3-electrode	2 M KOH	CV (5 $A \cdot g^{-1}$)	777.1	99.3% (3000 cycles)	[114] (2014)
rGO/$NiCo_2O_4$ composites by *in situ* assembly and thermal treatment	3-electrode	2 M KOH	CV (1 $A \cdot g^{-1}$)	1693	91.8% (2000 cycles)	[119] (2013)
3D mesoporous $NiCo_2O_4$-graphene hybrid by freeze drying and hydrothermal reaction	3-electrode	2 M KOH	CV (1 $A \cdot g^{-1}$)	778	90% (10000 cycles)	[120] (2014)
$MnMoO_4$/graphene composites	2-electrode	1 M Na_2SO_4	CV (2 $A \cdot g^{-1}$)	364	88% (1000 cycles)	[21] (2014)
a-GNS/NiAl-LDH via *in situ* growth of NiAl-LDH nanoflakes on a-GNS	2-electrode	6 M KOH	CV (0.1 $A \cdot g^{-1}$)	1730.2	99.2% (500 cycles)	[121] (2013)
3D sandwich structure graphene-NiAl-LDH via hydrothermal process	3-electrode	6 M KOH	CV (3.57 $A \cdot g^{-1}$)	1329	91% (500 cycles)	[116] (2014)
$FeNi_3$-graphene composites by thermal decomposition of LDH	3-electrode	6 M KOH	CV (10 $A \cdot g^{-1}$)	607	99% (1000 cycles)	[118] (2013)

improve the capacitance. The enhanced specific capacitance is attributed not only to the redox reactions of the heteroatom-containing functional groups (i.e., pseudocapacitance) but also to enhanced surface wettability of the electrode (i.e., reduced equivalent series resistance).[13, 122]

Of the chemical doping of carbon-based materials, nitrogen is considered to be an excellent candidate as its size and valence bonds are similar to those of carbon atoms. The incorporation of nitrogen group into the basal plane or edge of graphene sheets greatly improves the performance of graphene electrode.[13, 122, 123] Urea, hexamethylenetetramine and ammonia as well as organic amine have been used as the nitrogen source.[122–124] So far, several approaches have been reported for the synthesis of nitrogen-doped graphene (NG), such as nitrogen plasma,[123] thermal annealing treatment,[13] microwave synthesis,[124] arc-discharge, CVD and hydrothermal methods.[122, 125]

Among all these strategies, hydrothermal and solvothermal reactions are effective, facile and low costs. For example, Wang et al. produced NG under hydrothermal conditions by using common ammonium salts with hard acid-soft base pairs as nitrogen-doping agents.[122] They found that any ammonium salt with an amphoteric character could be used as an effective doping agent for the synthesis of NG. During the hydrothermal reaction, amphoteric salts gradually released NH_3 that continually reacted with the oxygen functional groups of GO, leading to doping of high-level nitrogen into the graphene skeleton. Moreover, the *in situ* produced reducing agent could further remove the oxygen functional groups on GO. That is, in this process, ammonium salt acted as both nitrogen-doping agent and reducing agent. The as-prepared NG exhibited remarkably enhanced electrochemical performance for SCs.

In another study, Lee et al. prepared NG by using GO and hexamethylenetetramine (HMT) as the precursors via a simple hydrothermal reaction. HMT plays an important role both as reducing agent and as doping agent for the GO, installing both nitrogen into the graphene sheets and removing oxygenated moieties from the surface as well.

Under hydrolytic conditions HMT has been known to release ammonia and hydroxide, and thus has the capacity to act as reducing agent for GO. The ammonia and hydroxide were involved in removing oxygenated functional groups from GO. Concurrently, the ammonia could also induce exchange with the carbon atoms within the lattice. Lee et al. prepared NG with a very significant nitrogen content (8.62 atom%) which featured a high specific capacitance. Various nitrogen species, such as pyridinic-N, pyrrolic-N, and quaternary-N, were detected and shown in Figure 25.[125]

From these studies, we can see that the nitrogen configurations and nitrogen content play crucial roles in determining the eventual capacitance. Proper configurations of nitrogen atoms and high nitrogen content are beneficial for increasing the electrical conductivity of NG and as a result improving the capacitance and other kinetic properties

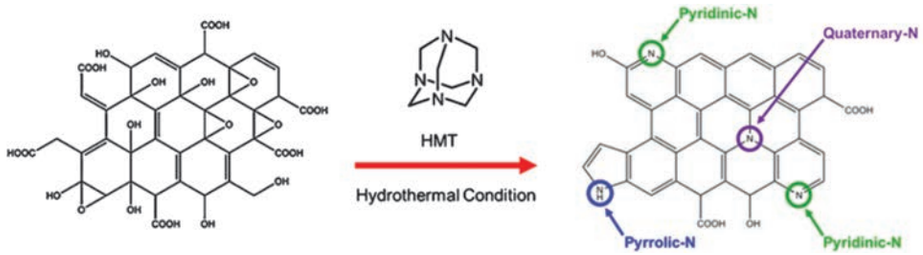

Fig. 25. Postulated route for NG-HMT. Reproduced with permission from [126], G. Luo, et al., *ACS Appl. Mater. Interfaces* 5, 11184 (**2013**). © 2012, Elsevier Ltd.

of SCs. There are three main arrangements of nitrogen in graphene, pyridinic-N, pyrrolic-N, and quaternary-N. Experimental and theoretical studies have shown that the pyridinic-N graphene has the strongest electron deficiency for accepting electrons and quaternary-N graphene exhibits a lowest diffusion and desorption barrier.[126, 127] Yang et al. synthesized NG using a microwave-assisted hydrothermal reaction. The ratio between nitrogen configurations was adjusted by controlling the reaction time to optimize SCs performance.[127] The authors attributed the enhanced electrical conductivity and SCs performances to its high concentration of quaternary-N. Gopalakrishnan et al. prepared heavily nitrogenated graphene oxide by microwave synthesis with urea as the nitrogen source, where the nitrogen concentration was controlled by the graphene to urea mass ratio. At the mass ratio of 1:1, the resulting NG exhibited the highest nitrogen content of 18.2 wt% and an outstanding performance for SCs.[124]

For the boron doped graphene, when boron is bonded within a graphene framework, it introduces a defect in the nearby sites because boron atom has only three valence electrons, and thereby induces uneven charge distribution, which can facilitate charge transfer and thus enhance their electrochemical performance.[29] For instance, Niu et al. preapred boron-doped graphene (BG) through the pyrolysis of GO with boric acid (H_3BO_3) in an argon atmosphere at 900 °C. When both boron-doping and reduction of GO were used simultaneously, H_3BO_3 was converted into boron oxide (B_2O_3) at high temperature accompanied by diffusing B_2O_3 vapor into the graphene nanosheets. The boron atoms could then replace the carbon atoms within the graphene layers and dope into the graphene lattice. The doping extent within the graphene reached a maximum of 4.7% after 3 h of pyrolysis, which directly affected the electrochemical properties of the material. The BG with the highest boron content exhibited the highest capacitive behavior (Fig. 26).[29] Han et al. produced BG on a large scale by refluxing reduction of GO in borane-tetrahydrofuran.[128] The obtained BG exhibited a high specific surface area and excellent SC performance, which was attributed to ion adsorption on the surface of BG in addition to electrochemical redox reactions (Table VIII).

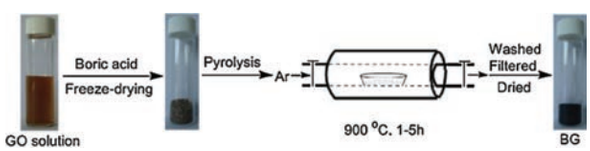

Fig. 26. Schematic illustration for the synthesis of the BG. Reproduced with permission from [29], L. Niu, et al., *Electrochim. Acta* 108, 666 (**2013**). © 2013, Elsevier Ltd., All rights reserved.

5. GRAPHENE-OTHER CARBON MATERIALS COMPOSITES

It is well known that, electrical conductivity and specific surface area are two critical factors for SCs. Hybrid structures based on graphene and other carbon materials as electrodes for energy storage application have attracted particular attention. Activated carbons, carbon fibers, carbon nanotubes (CNTs), carbon aerogels and porous carbons have all been used to prepare composites with graphene for SCs.[31, 130–133] In these composites, the graphene can not only provide vacancies to accommodate ions, but also enhance the bulk conductivity of composites, while the other carbon materials act as spacers to effectively prevent restacking of graphene and improve the specific surface area.

Among all carbon materials, only active carbon (AC) has been commercially used as SC electrode materials due to its high surface area and moderate costs. However, its application is strongly restricted by its low energy density and inferior rate capability due to relatively low conductivity.[130] Combination of AC with graphene will give rise to better performance due to the synergistic effects. Zheng et al. prepared porous graphene/AC nanosheet composites via hydrothermal carbonization and subsequent two-step chemical activation with KOH (Fig. 27).[130] Generally porous structures can be derived by chemical activation with KOH or NaOH.[134] In the obtained composites, a layer of porous AC is coated on graphene sheets, which not only inhibits agglomeration and increases the surface area, but also enhances packing density, which is of importance for practical applications as the space per power unit is always limited. On the other hand, integrating graphene into the AC matrix will notably increase the conductivity of the activated carbon.

Table VIII. Summary of SC performance for graphene/heteroatoms composites.

Preparation method or active material of electrode	Electrode configuration	Electrolyte	Measurement protocol	Maximum capacitance ($F \cdot g^{-1}$)	Capacitance retention	Ref. (year)
Nitrogen-doped graphene (NG) under hydrothermal by using amphoteric ammonium salt as nitrogen source	2-electrode	1 M KOH	CV (1 $A \cdot g^{-1}$)	242	97.6% (5000 cycles)	[122] (2014)
NG via pyrolysis of poly methyl methacrylate–GO composites in a mixed nitrogen and ammoniac	2-electrode	Ionic liquid $EMIMBF_4$	CV (1 $A \cdot g^{-1}$)	290.3	83.6% (1000 cycles)	[13] (2014)
NG produced via ammonia plasma treatment of GO	3-electrode	1 M H_2SO_4	CV (100 $mV \cdot s^{-1}$)	9.5 $mF \cdot cm^{-2}$	100% (700 cycles)	[123] (2014)
NG obtained using hydrothermal reaction with GO and hexamethylenetetramine	3-electrode	6 M KOH	CV (0.5 $A \cdot g^{-1}$)	161	98.1% (5000 cycles)	[125] (2012)
NG obtained by using microwave-assisted hydrothermal reaction	2-electrode	1 M $LiPF_6$	CV (0.1 $A \cdot g^{-1}$)	96.4	100% (1500 cycles)	[127] (2014)
Heavily nitrogenated GO by microwave synthesis with urea as the nitrogen source	2-electrode	6 M KOH	CV (5 $mV \cdot s^{-1}$)	461	97.3% (1000 cycles)	[124] (2013)
Boron-doped graphene (BG) prepared through pyrolysis of GO with H_3BO_3 in an argon atmosphere at 900 °C	2-electrode	6 M KOH	CV (0.5 $A \cdot g^{-1}$)	172.5	96.5% (5000 cycles)	[29] (2013)
BG prepared via the reduction of GO by a borane-tetrahydrofuran adduct under reflux	3-electrode	6 M KOH	CV (20 $mV \cdot s^{-1}$)	200	95% (4500 cycles)	[128] (2013)

The obtained graphene/AC nanosheet composite exhibits a high capacitance and excellent cycling stability. Continuous carbon nanofibers (CNF) synthesized by electrospinning carry high connectivity for electron transport and low electrical resistivity, and thus have attracted substantial interest. Dong et al. synthesized carbon nanofiber/graphene (CNF/G) composites by *in situ* electrospinning of polymer nanofibers with a simultaneous spray of graphene oxide through a final heat treatment.[131] They noted that the obtained CNF/G composite exhibited good specific capacitance, because the freestanding CNF web acted as a framework for supporting the graphene and helping to prevent the agglomeration of graphene and to provide high conductivity.

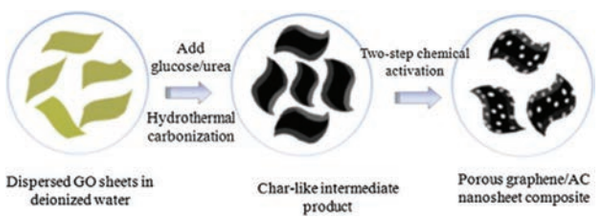

Fig. 27. Schematic illustration of the experimental steps in the preparation of porous graphene/AC nanosheet composites. Reproduced with permission from [130], C. Zheng, et al., *J. Power Sources* 258, 290 (**2014**). © 2014, Elsevier.

Carbon nanotubes (CNT) show very good properties for SCs, such as high surface area, good electrical conductivity and controlled pore size distribution. In the fabrication of graphene electrodes with multiwalled and single-walled carbon nanotubes, CNTs may be inserted into the interlayer space of graphene nanosheets. This can not only prevent agglomeration of the graphene sheets and increase the electrolyte-accessible surface area, but also reduce the internal electrical resistance. For example, Zhang et al. developed a single-walled carbon nanotubes/graphene composite with a high specific capacitance of 261 $F \cdot g^{-1}$.[22] Shakir fabricated a multiwalled CNTs-graphene hybrid film electrode using layer-by-layer (LBL) assembly. The resulted hybrid film electrode raised the energy density and power density as compared to that of bare graphene electrodes.[14] Jung et al. synthesized a chemically linked graphene-CNT composite with a lamellar structure via an amidation reaction. Because of the enlarged interlayer spacing, the composite generated

Table IX. Summary of SC performance for graphene/other carbon material composites.

Preparation method or active material of electrode	Electrode configuration	Electrolyte	Measurement protocol	Maximum capacitance ($F \cdot g^{-1}$)	Capacitance retention	Ref. (year)
Porous graphene/AC composite via hydrothermal carbonization and chemical activation with KOH	3-electrode	6 M KOH	CV (100 $mV \cdot s^{-1}$)	210	94.7% (5000 cycles)	[130] (2014)
Carbon nanofiber/graphene composite by *in situ* electrospinning and spraying GO, followed by heat treatment.	3-electrode	6 M KOH	CV (1 $A \cdot g^{-1}$)	183	92% (4500 cycles)	[131] (2013)
Graphene-single walled carbon nanotubes hybrid	2-electrode	Ionic liquid	CV (190 $mA \cdot g^{-1}$)	261	94% (10000 cycles)	[22] (2013)
Multiwalled CNTs-graphene hybrid film electrode using LBL assembly	3-electrode	1 M $LiClO_4$	CV (5 $mV \cdot s^{-1}$)	390	97% (25000 cycles)	[14] (2014)
Chemically linked graphene–CNT composite by amidation reaction	2-electrode	Organic electrolyte	CV (0.5 $A \cdot g^{-1}$)	165 $F \cdot cm^{-3}$	–	[31] (2013)
Porous carbon-graphene material via chemical process	3-electrode	6 M KOH	CV (0.5 $A \cdot g^{-1}$)	213.3	95.4% (1000 cycles)	[133] (2013)
Carbon aerogels-RGO composite films by directly blending	3-electrode	1 M KCl	CV (5 $mV \cdot s^{-1}$)	157	–	[132] (2013)

a high volumetric capacitance of 165 $F \cdot cm^{-3}$ for SCs (Table IX).[31]

6. GRAPHENE-BASED TERNARY COMPOSITES

From the above survey, we can see that each class of materials has its distinct advantages and disadvantages when used for SCs. For example, carbon materials have high stability but come with low specific capacitance; while transition metal oxides and conducting polymers have relatively high capacitance, but show relatively low mechanical stability and cycle life. The aforementioned graphene-based binary composites have exhibited higher specific capacitance than the individual components alone due to the synergistic effects. However, numerous studies show that the capacitor performance may be further increased by graphene-based ternary composites, such as graphene and other carbon materials, metal oxides, conducting polymers, as well as multicomponent composites.[25, 135, 136]

When integrating graphene with other carbon materials, metal oxides, conducting polymers, etc, the other materials usually act as spacers to prevent the agglomeration of graphene layers.[1, 135, 137] A second motivation is to provide more active sites for anchoring metal oxides or conducting polymers. Park et al. synthesized Co_3O_4-graphene-carbon black filler composites by ultrasonication and microwave-assisted methods.[135] The carbon black acted as a structural modifier forming conductive links among layered graphene and Co_3O_4 particles. Kim et al. fabricated a ternary hybrid based on MnO_2 nanoneedles-CNT-graphene sheets by using the direct paper dipping method.[137] CNTs intercalated between graphene layers preventing the restacking of graphene sheets, and MnO_2 nanoneedles formed on the outermost graphene layer maximizing the surface area, which improved the diffusion rate of electrolyte ions and facilitated the pseudo-capacitive reaction. Bai et al. preapred a rGO/CNT/NiO (GCN) composite, using urea to control the hydrolysis of metal salts

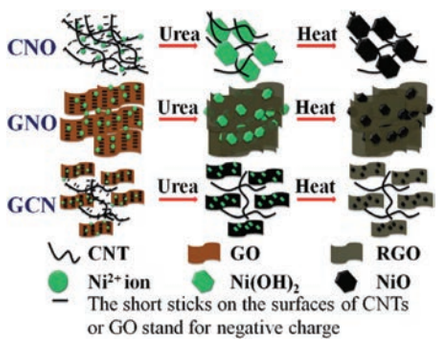

Fig. 28. Schematic illustrations of the synthesis process of CNT/NiO (CNO), RGO/NiO (GNO), and RGO/CNT/NiO (GCN) composite. Reproduced with permission from [1], Y. Bai, et al., *J. Mater. Chem. A* 2, 3834 **(2014)**. © 2014, Royal Society of Chemistry.

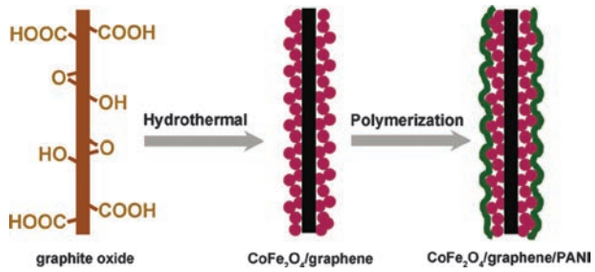

Fig. 29. Schematic illustration for the preparation of ternary CGP nanocomposites. Reproduced with permission from [140], P. Xiong, et al., *J. Power Sources* 245, 937 (**2014**). © 2013, Elsevier B.V.

and reduce GO to rGO.[1] CNTs inhibited the aggregation of rGO/NiO and improved the electron transport. Bai et al. ascribed this to the good conductivity of CNT (Fig. 28). GCN composites exhibited highly enhanced electrochemical performance.

Xu et al. prepared PANI-CNF-GO ternary composites via *in situ* polymerization.[16] The use of CNF drastically reduced the stacking interactions between GO sheets by delaminating them and opening pores into the CNF/GO architecture by *in situ* facile deposition of PANI. These authors inferred that the specific capacitance of the as-synthesized 3D hierarchical architecture might be further improved by reduction of GO before the deposition of PANI.

For the graphene-metal oxides-conducting polymers composites, the pseudo-capacitive contribution may be maximized with redox-active metal oxides and conducting polymers, with electrochemical double layer capacitive (EDLC) contributions from graphene. Han et al. prepared MnO_2-PPy-rGO ternary composites with a sandwich structure by a co-assembly approach.[139] The ternary composites exhibited excellent electrochemical performance compared to the individual components and their binary composites. The authors attributed the superior capacitance performance to the synergetic contribution of both conducting materials and the sandwich conductive network. Xiong et al. fabricated a ternary cobalt ferrite/graphene/PANI nanocomposite.[140] The authors ascribed the enhanced electrochemical performance to the particular laying of its nanostructure and synergistic effect between the individual components (Fig. 29).

In addition to the options discussed above, the metal oxides may be replaced by transition metals in the ternary nanocomposites. Giri et al. prepared graphene/Co/PANI composites by *in situ* oxidative polymerization of aniline.[141] They found that the incorporation of Co^{2+} ions within the PANI backbone resulted in increased conductivity. They believe that the mechanism was a narrower band gap which resulted in an increase of the specific capacitance.

Heteroatom-doped graphene has also been used to prepare composites with metal oxides to improve the electrical conductivity. For instance, NG may increase the electrical conductivity by introducing extra lone-pair electrons which strengthens the binding energy between NG and the metaloxide and reinforces the adsorption of electrolyte ions at the electrode surface. Zhao et al. synthesized nitrogen-doped graphene/Fe_2O_3 composites by a hydrothermal method.[136] The as-prepared composites show a better electrochemical performance than the graphene/Fe_2O_3 composites, as more nucleation sites were introduced by the nitrogen dopants (especially pyrrolic N) (Fig. 30, Table X).

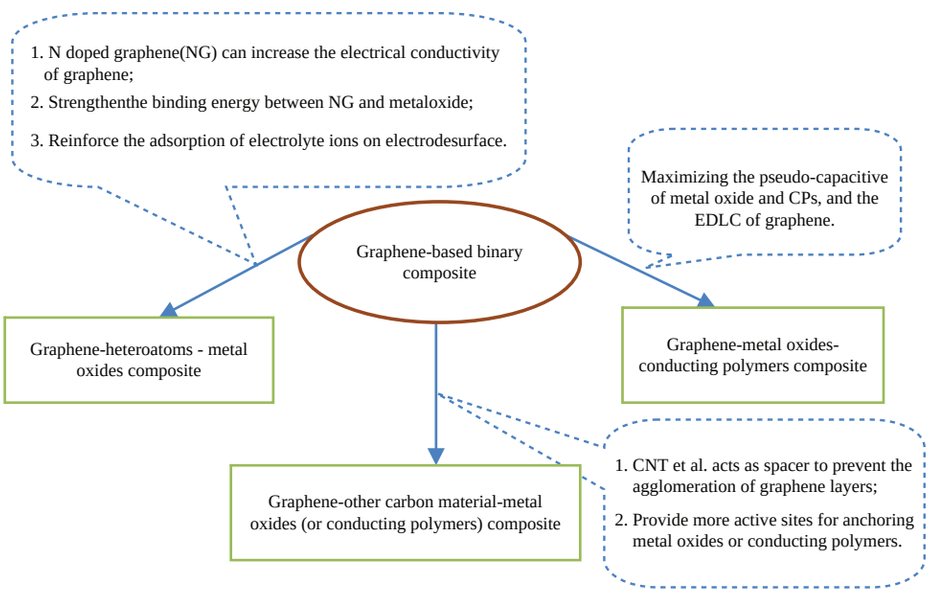

Fig. 30. Summary of key points for graphene-based binary composite for SCs.

REVIEW

Table X. Summary of SC performance for graphene-based ternary composites.

Preparation method or active material of electrode	Electrode configuration	Electrolyte	Measurement protocol	Maximum capacitance ($F \cdot g^{-1}$)	Capacitance retention	Ref. (year)
Co_3O_4-graphene-carbon blacks composites by ultrasonication and microwave	3-electrode	6 M KOH	CV (10 $mV \cdot s^{-1}$)	314	89% (1000 cycles)	[135] (2013)
MnO_2 nanoneedles-CNT-graphene sheets ternary hybrid using the direct paper dipping method	3-electrode	1 M Na_2SO_4	CV (10 $mV \cdot s^{-1}$)	367.23	84.6% (1000 cycles)	[137] (2014)
RGO/CNT/NiO composite, using urea to control the hydrolysis of metal salts and reduce GO to RGO	3-electrode	2 M KOH	CV (1 $A \cdot g^{-1}$)	1180	95% (2000 cycles)	[1] (2014)
Ni–Al LDH, CNT, and RGO ternary nanocomposite by one-step ethanol solvothermal	3-electrode	6 M KOH	5 $mA \cdot cm^{-2}$	1562	96.5% (1000 cycles)	[17] (2013)
Layer by layer assembly of ultrathin V_2O_5 anchored MWCNTs and graphene on textile fabrics	3-electrode	$LiClO_4$	CV (1 $mV \cdot s^{-1}$)	2590	97% (5000 cycles)	[142] (2014)
RuO_2 anchored graphene and CNT hybrid Foam via CVD and dip-coating	2-electrode	2 M Li_2SO_4	CV (10 $mV \cdot s^{-1}$)	502.78	106% (8100 cycles)	[143] (2014)
PANI-CNF-GO ternary composites via *in situ* polymerization	2-electrode	1 M H_2SO_4	CV (10 $mV \cdot s^{-1}$)	450.2	90.2% (1000 cycles)	[16] (2014)
MnO_2 nanorods-PANI-GO ternary composites	3-electrode	1 M Na_2SO_4	CV (0.25 $A \cdot g^{-1}$)	512	97% (5000 cycles)	[18] (2014)
MnO_2-PPy-graphene ternary composites	3-electrode	1 M Na_2SO_4	CV (0.25 $A \cdot g^{-1}$)	404	91% (5000 cycles)	[139] (2014)
Ternary cobalt ferrite/graphene/PANI nanocomposite	3-electrode	1 MKOH	CV (1 $mV \cdot s^{-1}$)	1133.3	96% (5000 cycles)	[140] (2014)
Growth vertically aligned tunable PANI on graphene/ZrO_2 nanocomposites	3-electrode	1 M H_2SO_4	CV (1 $mV \cdot s^{-1}$)	1359.99	93.02% (1000 cycles)	[144] (2014)
Graphene/Co/PANI composites by *in situ* oxidative polymerization of aniline	3-electrode	6 M KOH	CV (2 $mV \cdot s^{-1}$)	989	79% (1000 cycles)	[141] (2013)
Nitrogen-doped graphene/Fe_2O_3 composites by hydrothermal method	3-electrode	1 M Na_2SO_4	CV (2 $A \cdot g^{-1}$)	260.1	82.5% (1000 cycles)	[136] (2014)

7. CONCLUSION AND PERSPECTIVES

As presented above, combination of graphene with metal oxides, conducting polymers, heteroatoms or other carbon materials is important in the preparation of high-performance SCs. These binary or ternary composites generate improved electrochemical properties as compared to pristine graphene. Although much progress has been made, the specific capacitance, cycle stability and rate capability will still have to be further improved for practical applications. Some critical issues remain for further studies:

(1) Although synergistic strategies are emerging, exquisite synthesis strategies are still needed, since the performance of SCs is strongly influenced by the morphology and microstructure of the electrode materials. Rational design and synthesis of graphene-based composites with a precise control of their compositions, morphologies and hierarchical structures is of vital importance for high-performance SCs.

(2) The interaction mechanism between graphene and other ingredients needs to be clarified. A great many researchers attribute the outstanding properties of graphene-based composites to the synergistic effects among the components. However, because the contact between graphene and other components is usually electrostatic or physical adsorption in nature, the bonding force is weak. This leads to poor conductivity and mechanical stability of the electrode. Therefore it is still a challenge to synthesize mechanically robust composites.
(3) The techniques for the preparation of electrodes with graphene-based composites need to be further improved, in particular, control of the thickness of electrode materials, use of conducting substrates, and self-supporting electrodes to replace binder and conductive adhesives. Further research is urgently needed for the optimization of SC performance.

Acknowledgments: This work was supported, in part, by the National Science Foundation (CHE-1265635 and DMR-1409396) and by the Research Foundation of Chongqing University of Science and Technology (CK2014Z17).

REVIEW

References and Notes

1. Y. Bai, M. Du, J. Chang, J. Sun, and L. Gao, *J. Mater. Chem. A* 2, 3834 (**2014**).
2. Y. B. Tan and J.-M. Lee, *J. Mater. Chem. A* 1, 14814 (**2013**).
3. W.-Y. Tsai, R. Lin, S. Murali, L. Li Zhang, J. K. McDonough, R. S. Ruoff, P.-L. Taberna, Y. Gogotsi, and P. Simon, *Nano Energy* 2, 403 (**2013**).
4. Z. Lei, Z. Liu, H. Wang, X. Sun, L. Lu, and X. S. Zhao, *J. Mater. Chem. A* 1, 2313 (**2013**).
5. J. Cao, Y. Wang, Y. Zhou, J.-H. Ouyang, D. Jia, and L. Guo, *J. Electroanal. Chem.* 689, 201 (**2013**).
6. J. Chang, M. Jin, F. Yao, T. H. Kim, V. T. Le, H. Yue, F. Gunes, B. Li, A. Ghosh, S. Xie, and Y. H. Lee, *Adv. Funct. Mater.* 23, 5074 (**2013**).
7. J. Shen, C. Yang, X. Li, and G. Wang, *ACS Appl. Mater. Interfaces* 5, 8467 (**2013**).
8. B. Li, Y. Fu, H. Xia, and X. Wang, *Mater. Lett.* 122, 193 (**2014**).
9. H. Wang, H. Yi, X. Chen, and X. Wang, *J. Mater. Chem. A* 2, 3223 (**2014**).
10. N. Ashok Kumar and J. B. Baek, *Chem. Commun.* 50, 6298 (**2014**).
11. Q. Cheng, J. Tang, N. Shinya, and L.-C. Qin, *Sci. Technol. Adv. Mater.* 15, 014206 (**2014**).
12. B. You, N. Li, H. Zhu, X. Zhu, and J. Yang, *ChemSusChem.* 6, 474 (**2013**).
13. V. H. Pham, T.-D. Nguyen-Phan, J. Jang, T. D. Tuyet Vu, Y. J. Lee, I. K. Song, E. W. Shin, and J. S. Chung, *RSC Adv.* 4, 22455 (**2014**).
14. I. Shakir, *Electrochim. Acta* 129, 396 (**2014**).
15. A. Sumboja, C. Y. Foo, X. Wang, and P. S. Lee, *Adv. Mater.* 25, 2809 (**2013**).
16. D. Xu, Q. Xu, K. Wang, J. Chen, and Z. Chen, *ACS Appl. Mater. Interfaces* 6, 200 (**2014**).
17. W. Yang, Z. Gao, J. Wang, J. Ma, M. Zhang, and L. Liu, *ACS Appl. Mater. Interfaces* 5, 5443 (**2013**).
18. G. Han, Y. Liu, L. Zhang, E. Kan, S. Zhang, J. Tang, and W. Tang, *Sci. Rep.* 4, 4824 (**2014**).
19. Y. Zhang, M. Ma, J. Yang, W. Huang, and X. Dong, *RSC Adv.* 4, 8466 (**2014**).
20. P. Yu, Y. Li, X. Zhao, L. Wu, and Q. Zhang, *Langmuir* 30, 5306 (**2014**).
21. D. Ghosh, S. Giri, M. Moniruzzaman, T. Basu, M. Mandal, and C. K. Das, *Dalton Trans.* 43, 11067 (**2014**).
22. F. Zhang, J. Tang, N. Shinya, and L.-C. Qin, *Chem. Phys. Lett.* 584, 124 (**2013**).
23. G. S. Gund, D. P. Dubal, B. H. Patil, S. S. Shinde, and C. D. Lokhande, *Electrochim. Acta* 92, 205 (**2013**).
24. Z.-F. Li, H. Zhang, Q. Liu, Y. Liu, L. Stanciu, and J. Xie, *Carbon* 71, 257 (**2014**).
25. Y. S. Lim, Y. P. Tan, H. N. Lim, N. M. Huang, W. T. Tan, M. A. Yarmo, and C.-Y. Yin, *Ceram. Int.* 40, 3855 (**2014**).
26. W. Deng, W. Lan, Y. Sun, Q. Su, and E. Xie, *Appl. Surf. Sci.* 305, 433 (**2014**).
27. M. Kim, Y. Hwang, and J. Kim, *J. Power Sources* 239, 225 (**2013**).
28. T. Liu, G. Shao, and M. Ji, *Mater. Lett.* 122, 273 (**2014**).
29. L. Niu, Z. Li, W. Hong, J. Sun, Z. Wang, L. Ma, J. Wang, and S. Yang, *Electrochim. Acta* 108, 666 (**2013**).
30. H. Cao, X. Zhou, Z. Qin, and Z. Liu, *Carbon* 56, 218 (**2013**).
31. N. Jung, S. Kwon, D. Lee, D. M. Yoon, Y. M. Park, A. Benayad, J. Y. Choi and J. S. Park, *Adv. Mater.* 25, 6854 (**2013**).
32. H. Yadegari, H. Heli, and A. Jabbari, *J. Solid State Electrochem.* 17, 2203 (**2013**).
33. J. P. C. Trigueiro, R. L. Lavall, and G. G. Silva, *J. Power Sources* 256, 264 (**2014**).
34. H. Cao, X. Zhou, Y. Zhang, L. Chen, and Z. Liu, *J. Power Sources* 243, 715 (**2013**).
35. Q. Wang, J. Yan, Z. Fan, T. Wei, M. Zhang, and X. Jing, *J. Power Sources* 247, 197 (**2014**).
36. L. Wang, Y. Ye, X. Lu, Z. Wen, Z. Li, H. Hou, and Y. Song, *Sci. Rep.* 3, 3568 (**2013**).
37. Z. Gao, W. Yang, J. Wang, B. Wang, Z. Li, Q. Liu, M. Zhang, and L. Liu, *Energy Fuels* 27, 568 (**2013**).
38. Y. Meng, K. Wang, Y. Zhang, and Z. Wei, *Adv. Mater.* 25, 6985 (**2013**).
39. Z. F. Li, H. Zhang, Q. Liu, L. Sun, L. Stanciu, and J. Xie, *ACS Appl. Mater. Interfaces* 5, 2685 (**2013**).
40. S. B. Kulkarni, U. M. Patil, I. Shackery, J. S. Sohn, S. Lee, B. Park and S. Jun, *J. Mater. Chem. A* 2, 4989 (**2014**).
41. H.-P. Cong, X.-C. Ren, P. Wang, and S.-H. Yu, *Energy Environ. Sci.* 6, 1185 (**2013**).
42. B. Mu, W. Zhang, and A. Wang, *J. Nanopart. Res.* 16, 2432 (**2014**).
43. H. Liu, Y. Wang, X. Gou, T. Qi, J. Yang, and Y. Ding, *Mater. Sci. Eng. B* 178, 293 (**2013**).
44. L. Li, X. Zhang, J. Qiu, B. L. Weeks, and S. Wang, *Nano Energy* 2, 628 (**2013**).
45. Y. Liu, Y. Ma, S. Guang, H. Xu, and X. Su, *J. Mater. Chem. A* 2, 813 (**2014**).
46. S. Xiong, Y. Shi, J. Chu, M. Gong, B. Wu, and X. Wang, *Electrochim. Acta* 127, 139 (**2014**).
47. Q. Zhang, Y. Li, Y. Feng, and W. Feng, *Electrochim. Acta* 90, 95 (**2013**).
48. D. Gui, C. Liu, F. Chen, and J. Liu, *Appl. Surf. Sci.* 307, 172 (**2014**).
49. Y. Luo, D. Kong, Y. Jia, J. Luo, Y. Lu, D. Zhang, K. Qiu, C. M. Li, and T. Yu, *RSC Adv.* 3, 5851 (**2013**).
50. W. Fan, C. Zhang, W. W. Tjiu, K. P. Pramoda, C. He, and T. Liu, *ACS Appl. Mater. Interfaces* 5, 3382 (**2013**).
51. A. K. Sarker and J.-D. Hong, *Colloids Surf. A* 436, 967 (**2013**).
52. P. A. Basnayaka, M. K. Ram, L. Stefanakos, and A. Kumar, *Mater. Chem. Phys.* 141, 263 (**2013**).
53. P. A. Basnayaka, M. K. Ram, E. K. Stefanakos, and A. Kumar, *Electrochim. Acta* 92, 376 (**2013**).
54. J. Li, H. Xie, and Y. Li, *Mater. Lett.* 124, 215 (**2014**).
55. Y. Liu, Y. Zhang, G. Ma, Z. Wang, K. Liu, and H. Liu, *Electrochim. Acta* 88, 519 (**2013**).
56. T. Qian, C. Yu, S. Wu, and J. Shen, *J. Mater. Chem. A* 1, 6539 (**2013**).

57. A. Gupta, A. J. Akhtar, and S. K. Saha, *Mater. Chem. Phys.* 140, 616 (**2013**).
58. S. Sahoo, S. Dhibar, G. Hatui, P. Bhattacharya, and C. K. Das, *Polymer* 54, 1033 (**2013**).
59. Z. Chen, D. Yu, W. Xiong, P. Liu, Y. Liu, and L. Dai, *Langmuir* 30, 3567 (**2014**).
60. X. Wang, T. Wang, C. Yang, H. Li, and P. Liu, *Appl. Surf. Sci.* 287, 242 (**2013**).
61. Y. Zhao, J. Liu, Y. Hu, H. Cheng, C. Hu, C. Jiang, L. Jiang, A. Cao, and L. Qu, *Adv. Mater.* 25, 591 (**2013**).
62. D. Sun, L. Jin, Y. Chen, J.-R. Zhang, and J.-J. Zhu, *ChemPlusChem.* 78, 227 (**2013**).
63. W. Cai, T. Lai, W. Dai, and J. Ye, *J. Power Sources* 255, 170 (**2014**).
64. H. Song, X. Li, Y. Zhang, H. Wang, H. Li, and J. Huang, *Ceram. Int.* 40, 1251 (**2014**).
65. X. Liu, X. Qi, Z. Zhang, L. Ren, Y. Liu, L. Meng, K. Huang, and J. Zhong, *Ceram. Int.* 40, 8189 (**2014**).
66. C. Zhang, H. Zhou, X. Yu, D. Shan, T. Ye, Z. Huang, and Y. Kuang, *RSC Adv.* 4, 11197 (**2014**).
67. A. T. Chidembo, S. H. Aboutalebi, K. Konstantinov, C. J. Jafta, H. K. Liu, and K. I. Ozoemena, *RSC Adv.* 4, 886 (**2014**).
68. Z. Li, J. Wang, L. Niu, J. Sun, P. Gong, W. Hong, L. Ma, and S. Yang, *J. Power Sources* 245, 224 (**2014**).
69. S. Chen, J. Duan, Y. Tang, and S. Zhang Qiao, *Chemistry* 19, 7118 (**2013**).
70. G. Lee, Y. Cheng, C. V. Varanasi, and J. Liu, *J. Phys. Chem. C* 118, 2281 (**2014**).
71. K. Subramani, D. Jeyakumar, and M. Sathish, *Phys. Chem. Chem. Phys.* 16, 4952 (**2014**).
72. T. Liu, G. Shao, M. Ji, and Z. Ma, *Ionics* 20, 145 (**2013**).
73. Y. Liu, D. Yan, R. Zhuo, S. Li, Z. Wu, J. Wang, P. Ren, P. Yan, and Z. Geng, *J. Power Sources* 242, 78 (**2013**).
74. J. Ge, H.-B. Yao, W. Hu, X.-F. Yu, Y.-X. Yan, L.-B. Mao, H.-H. Li, S.-S. Li, and S.-H. Yu, *Nano Energy* 2, 505 (**2013**).
75. M. Kim, Y. Hwang, and J. Kim, *Chem. Eng. J.* 230, 482 (**2013**).
76. Y. Liu, D. Yan, Y. Li, Z. Wu, R. Zhuo, S. Li, J. Feng, J. Wang, P. Yan, and Z. Geng, *Electrochim. Acta* 117, 528 (**2014**).
77. M. Kim, Y. Hwang, K. Min, and J. Kim, *Phys. Chem. Chem. Phys.: PCCP* 15, 15602 (**2013**).
78. A. K. Mondal, B. Wang, D. Su, Y. Wang, S. Chen, X. Zhang, and G. Wang, *Mater. Chem. Phys.* 143, 740 (**2014**).
79. Y. Xiao, Y. Cao, Y. Gong, A. Zhang, J. Zhao, S. Fang, D. Jia, and F. Li, *J. Power Sources* 246, 926 (**2014**).
80. M. Kim, Y. Hwang, and J. Kim, *J. Mater. Sci.* 48, 7652 (**2013**).
81. L. Wang, D. Deng, and K. Y. S. Ng, *J. Mater. Sci.* 48, 6410 (**2013**).
82. X. Feng, N. Chen, Y. Zhang, Z. Yan, X. Liu, Y. Ma, Q. Shen, L. Wang, and W. Huang, *J. Mater. Chem. A* 2, 9178 (**2014**).
83. M.-T. Lee, C.-Y. Fan, Y.-C. Wang, H.-Y. Li, J.-K. Chang, and C.-M. Tseng, *J. Mater. Chem. A* 1, 3395 (**2013**).
84. L. Li, Z. Hu, Y. Yang, P. Liang, A. Lu, H. Xu, Y. Hu, and H. Wu, *Chin. J. Chem.* 31, 1290 (**2013**).
85. S. Wu, W. Chen, and L. Yan, *J. Mater. Chem. A* 2, 2765 (**2014**).
86. C. C. Wang, H. C. Chen, and S. Y. Lu, *Chemistry* 20, 517 (**2014**).
87. Y. He, W. Chen, X. Li, Z. Zhang, J. Fu, C. Zhao, and E. Xie, *Acs Nano* 7, 174 (**2013**).
88. K.-H. Ye, Z.-Q. Liu, C.-W. Xu, N. Li, Y.-B. Chen, and Y.-Z. Su, *Inorg. Chem. Commun.* 30, 1 (**2013**).
89. M. Sawangphruk, P. Srimuk, P. Chiochan, A. Krittayavathananon, S. Luanwuthi, and J. Limtrakul, *Carbon* 60, 109 (**2013**).
90. L. Peng, X. Peng, B. Liu, C. Wu, Y. Xie, and G. Yu, *Nano lett.* 13, 2151 (**2013**).
91. Y. Fan, X. Zhang, Y. Liu, Q. Cai, and J. Zhang, *Mater. Lett.* 95, 153 (**2013**).
92. L. Wang, X. Li, T. Guo, X. Yan, and B. K. Tay, *Int. J. Hydrogen Energy* 39, 7876 (**2014**).
93. W. Zhou, X. Cao, Z. Zeng, W. Shi, Y. Zhu, Q. Yan, H. Liu, J. Wang, and H. Zhang, *Energy Environ. Sci.* 6, 2216 (**2013**).
94. M. Zhou, H. Chai, D. Jia, and W. Zhou, *New J Chem* 38, 2320 (**2014**).
95. G.-J. Liu, L.-Q. Fan, F.-D. Yu, J.-H. Wu, L. Liu, Z.-Y. Qiu, and Q. Liu, *J. Mater. Sci.* 48, 8463 (**2013**).
96. R. Ramachandran, S. Felix, M. Saranya, C. Santhosh, V. Velmurugan, B. P. C. Ragupathy, S. K. Jeong, and A. N. Grace, *IEEE Trans. Nanotechnol.* 12, 985 (**2013**).
97. R. Ramachandran, M. Saranya, C. Santhosh, V. Velmurugan, B. P. C. Raghupathy, S. K. Jeong, and A. N. Grace, *RSC Adv.* 4, 21151 (**2014**).
98. D. Ghosh, S. Giri, and C. K. Das, *ACS Sustainable Chem. Eng.* 1, 1135 (**2013**).
99. K. K. Purushothaman, B. Saravanakumar, I. M. Babu, B. Sethuraman, and G. Muralidharan, *RSC Adv.* 4, 23485 (**2014**).
100. W. Yang, Z. Gao, J. Wang, B. Wang, and L. Liu, *Solid State Sci.* 20, 46 (**2013**).
101. T. Qi, J. Jiang, H. Chen, H. Wan, L. Miao, and L. Zhang, *Electrochim. Acta* 114, 674 (**2013**).
102. Y.-Z. Liu, Y.-F. Li, Y.-G. Yang, Y.-F. Wen, and M.-Z. Wang, *Scr. Mater.* 68, 301 (**2013**).
103. S. D. Perera, A. D. Liyanage, N. Nijem, J. P. Ferraris, Y. J. Chabal and K. J. Balkus, *J. Power Sources* 230, 130 (**2013**).
104. Y. Cai, Y. Wang, S. Deng, G. Chen, Q. Li, B. Han, R. Han, and Y. Wang, *Ceram. Int.* 40, 4109 (**2014**).
105. S. P. Lim, N. M. Huang, and H. N. Lim, *Ceram. Int.* 39, 6647 (**2013**).
106. X. Xia, W. Lei, Q. Hao, W. Wang, and X. Wang, *Electrochim. Acta* 99, 253 (**2013**).
107. F. Zhang, D. Zhu, X. Chen, X. Xu, Z. Yang, C. Zou, K. Yang, and S. Huang, *Phys. Chem. Chem. Phys.* 16, 4186 (**2014**).
108. C. Jiang, B. Zhan, C. Li, W. Huang, and X. Dong, *RSC Adv.* 4, 18080 (**2014**).
109. Z. Wu, X. L. Huang, Z. L. Wang, J. J. Xu, H. G. Wang, and X. B. Zhang, *Sci. Rep.* 4, 3669 (**2014**).
110. H. Zhang, X. Yu, D. Guo, B. Qu, M. Zhang, Q. Li, and T. Wang, *ACS Appl. Mater. Interfaces* 5, 7335 (**2013**).
111. Q. Zhang, C. Xu, and B. Lu, *Electrochim. Acta* 132, 180 (**2014**).
112. H. Huang, L. Xu, Y. Tang, S. Tang, and Y. Du, *Nanoscale* 6, 2426 (**2014**).
113. G. He, L. Wang, H. Chen, X. Sun, and X. Wang, *Mater. Lett.* 98, 164 (**2013**).
114. Y. Luo, H. Zhang, D. Guo, J. Ma, Q. Li, L. Chen, and T. Wang, *Electrochim. Acta* 132, 332 (**2014**).
115. S. G. Hwang, J. E. Hong, G. O. Kim, H. M. Jeong, and K. S. Ryu, *ECS Solid State Lett.* 2, M8 (**2012**).
116. J. Xu, S. Gai, F. He, N. Niu, P. Gao, Y. Chen, and P. Yang, *J. Mater. Chem. A* 2, 1022 (**2014**).
117. J. Memon, J. Sun, D. Meng, W. Ouyang, M. A. Memon, Y. Huang, S. Yan, and J. Geng, *J. Mater. Chem. A* 2, 5060 (**2014**).
118. G. Abellán, E. Coronado, C. Martí-Gastaldo, A. Ribera, and T. F. Otero, *Part. Part. Sys. Char.* 30, 853 (**2013**).
119. L. Wang, X. Wang, X. Xiao, F. Xu, Y. Sun, and Z. Li, *Electrochim. Acta* 111, 937 (**2013**).
120. Y. Wei, S. Chen, D. Su, B. Sun, J. Zhu, and G. Wang, *J. Mater. Chem. A* 2, 8103 (**2014**).
121. N. Yulian, L. Ruiyi, L. Zaijun, F. Yinjun, and L. Junkang, *Electrochim. Acta* 94, 360 (**2013**).
122. D. Wang, Y. Min, Y. Yu, and B. Peng, *J. Colloid Interface Sci.* 417, 270 (**2014**).
123. H. Nolan, B. Mendoza-Sanchez, N. Ashok Kumar, N. McEvoy, S. O'Brien, V. Nicolosi, and G. S. Duesberg, *Phys. Chem. Chem. Phys.* 16, 2280 (**2014**).
124. K. Gopalakrishnan, A. Govindaraj, and C. N. R. Rao, *J. Mater. Chem. A* 1, 7563 (**2013**).

REVIEW

125. J. W. Lee, J. M. Ko, and J.-D. Kim, *Electrochim. Acta* 85, 459 **(2012)**.
126. G. Luo, L. Liu, J. Zhang, G. Li, B. Wang, and J. Zhao, *ACS Appl. Mater. Interfaces* 5, 11184 **(2013)**.
127. J. Yang, M. R. Jo, M. Kang, Y. S. Huh, H. Jung, and Y.-M. Kang, *Carbon* 73, 106 **(2014)**.
128. J. Han, L. L. Zhang, S. Lee, J. Oh, K.-S. Lee, J. R. Potts, J. Ji, X. Zhao, R. S. Ruoff, and S. Park, *Acs Nano* 7, 19 **(2013)**.
129. J. M. Bai, L. Zhang, R. P. Liang, and J. D. Qiu, *Chemistry* 19, 3822 **(2013)**.
130. C. Zheng, X. Zhou, H. Cao, G. Wang, and Z. Liu, *J. Power Sources* 258, 290 **(2014)**.
131. Q. Dong, G. Wang, H. Hu, J. Yang, B. Qian, Z. Ling, and J. Qiu, *J. Power Sources* 243, 350 **(2013)**.
132. C. Nie, D. Liu, L. Pan, Y. Liu, Z. Sun, and J. Shen, *Solid State Ionics* 247–248, 66 **(2013)**.
133. M. Li, J. Ding, and J. Xue, *J. Mater. Chem. A* 1, 7469 **(2013)**.
134. T. Kim, G. Jung, S. Yoo, K. S. Suh, and R. S. Ruoff, *Acs Nano* 7, 6899 **(2013)**.
135. S. Park and S. Kim, *Electrochim. Acta* 89, 516 **(2013)**.
136. P. Zhao, W. Li, G. Wang, B. Yu, X. Li, J. Bai, and Z. Ren, *J. Alloys Comp.* 604, 87 **(2014)**.
137. M. Kim, Y. Hwang, and J. Kim, *Phys. Chem. Chem. Phys.* 16, 351 **(2014)**.
138. Y. Joseph, I. Besnard, M. Rosenberger, B. Guse, H.-G. Nothofer, J. M. Wessels, U. Wild, A. Knop-Gericke, D. Su, R. Schlo1gl, A. Yasuda, and A. T. Vossmeyer, *J. Phys. Chem. B* 107, 7406 **(2003)**.
139. G. Han, Y. Liu, E. Kan, J. Tang, L. Zhang, H. Wang, and W. Tang, *RSC Adv.* 4, 9898 **(2014)**.
140. P. Xiong, H. Huang, and X. Wang, *J. Power Sources* 245, 937 **(2014)**.
141. S. Giri, D. Ghosh, and C. K. Das, *J. Electroanal. Chem.* 697, 32 **(2013)**.
142. I. Shakir, Z. Ali, J. Bae, J. Park, and D. J. Kang, *Nanoscale* 6, 4125 **(2014)**.
143. W. Wang, S. Guo, I. Lee, K. Ahmed, J. Zhong, Z. Favors, F. Zaera, M. Ozkan, and C. S. Ozkan, *Sci. Rep.* 4, 4452 **(2014)**.
144. S. Giri, D. Ghosh, and C. K. Das, *Adv. Funct. Mater.* 24, 1312 **(2014)**.

REVIEW